NONLINEAR ANALYSIS OF REINFORCED CONCRETE SHEAR WALL STRUCTURES

Trevor Kelly[1]

ABSTRACT

Although shear walls are a widely used system for providing lateral load resistance, nonlinear analysis procedures for this type of element are much less well developed than those for frame and truss elements. Equivalent flexural models do not include shear deformation and are only suited for symmetric, straight walls. This paper describes the development of an analysis model which includes nonlinear effects for both shear and flexure. The formulation is based on a "macro" modelling approach which is suitable for complete building models in a design office environment.

An analysis methodology is developed using engineering mechanics and experimental results and implemented in an existing nonlinear analysis computer program. A model is developed and validated against test results of solid walls and walls with openings. This shows that the model can capture the general characteristics of hysteretic response and the maximum strength of the wall. Results can be evaluated using acceptance criteria derived from published guidelines. An example shear wall building is then evaluated using both the nonlinear static and the nonlinear dynamic procedures. The procedure is shown to be a practical method for implementing performance based design procedures for shear wall buildings.

Keywords: Cantilever shear walls, reinforced concrete, nonlinear analysis, capacity curve, pushover analysis, hysteresis, earthquake, performance based design.

1 INTRODUCTION

Reinforced concrete shear walls form a widely used class of components for resisting lateral loads in building systems. Although a symmetric layout of prismatic walls represents the ideal from a structural engineering perspective, there are often architectural and functional requirements which result in wall configurations which are non-symmetric, non-prismatic and with irregularly placed openings. There are few practical tools available for assessing the performance of these types of walls beyond the elastic range.

Our profession is moving to implement performance based design and evaluation, the objective of which is to accurately assess the seismic performance of buildings. This requires that the structural system be evaluated beyond the elastic range, using nonlinear analysis techniques. For highly nonlinear systems the load distributions change after yielding and a time history analysis is the only analysis technique which will capture this feature of response.

Past studies of the nonlinear response of shear wall structures, some of which have formed the basis for our current codes [1], have been based on the use of equivalent flexural elements. These "equivalent columns" are still the most common approach used [2]. However, they have severe limitations in that they do not incorporate shear cracking, are difficult to implement for walls with openings and do not represent the asymmetrical response of walls which are not symmetric, such as C and L shaped walls.

Design procedures for irregular shear walls are often based on strut and tie models and there have been attempts to incorporate these models into structural analysis programs [3]. There is now at least one commercially available program including a general wall model based on strut and tie representation [4]. These models indicate promise for evaluating shear wall structures but input preparation is complex and the resulting model has a large number of degrees of freedom and elements. With currently available computer hardware they are more suited for the study of individual components rather than complete structures, or for nonlinear static rather than dynamic analyses.

There are a number of aspects of the seismic response of yielding shear walls structures which would be better understood by a more accurate assessment. These include:

1. A dynamic magnification factor, ω_v, is applied to cantilever shear wall shear forces (C4.4.6.2 of NZS3101 [5]). This factor is based on limited studies of cantilever walls and its applicability to other wall configurations is not clear.

2. Linear elastic analyses of combined frame/wall systems produce reversed shear distributions (opposite sign of

[1]*Technical Director, Holmes Consulting Group, Auckland (Member).*

3. forces in the frame and wall) due to incompatible deformed shapes of the two systems. This is likely to change when yield occurs in either or both systems and the deformed shapes become more compatible.

4. Shear wall yield displacement is related to strength as well as section properties. Linear elastic models produce a stiffness proportional to section size, ignoring strength.

This paper describes an alternative procedure for modelling concrete shear walls, using a combination of plane stress elements to represent the shear properties of the walls and pairs of gap and truss elements to represent respectively the compression block and flexural reinforcing of the wall.

The modelling procedure is formulated using a combination of engineering mechanics and empirical data from tests on reinforced concrete shear walls. A model of an example wall is developed to check that the stiffness and strength characteristics conform with expected properties.

The model is validated by comparing predicted strength, stiffness and cyclic hysteresis properties with values from experimental data. From these results, a number of modelling and evaluation parameters are discussed. The formulation is then illustrated by evaluating the performance of a complete building.

2 MODELLING PROCEDURE

For linear elastic analysis, shear walls are generally modelled using either equivalent frame elements or, more often, using two dimensional elements, either plate or plane stress elements. For nonlinear analysis, shear walls may be modelled as frame elements as for elastic analysis, by strut and tie models or by detailed fibre models. The use of plate or plane stress elements is rare because of the difficulty in representing the yield function of a shear wall within this type of element.

The procedure described in this paper uses a combination of plane stress elements, to represent shear behaviour, and pairs of gap/truss elements to represent flexural behaviour. The aim was to develop a procedure which could be used for both static and dynamic nonlinear analysis of complete building systems. Whole building models are complex systems and so the formulation is based on *macro* modelling, rather than classical finite element modelling.

In macro modelling, wall elements are defined using a relatively coarse mesh, generally restricted to the refinement required to define the wall geometry. This differs from more general finite element analysis in that the wall segments are not sub-divided into portions small enough to accurately model stress distributions. Figure 1 shows the two types of model of the same wall segment.

The use of large macro elements reduces the size of the model and the resources required to perform nonlinear analyses. This is the type of modelling of shear walls used in design office analysis, for example using programs such as ETABS [6]. The macro approach also tends to be numerically more stable as there are less yielding events. However, there are two consequences of this simplification:

1. The large elements represent the overall response of a unit. The properties of these elements need to be based on empirical rules as well as engineering mechanics. This requires some characteristics to be derived from experimental evidence.

2. Not all failure states are checked as part of the element response calculations (for example, buckling or bond loss) and so further empirical rules are applied to results to evaluate performance.

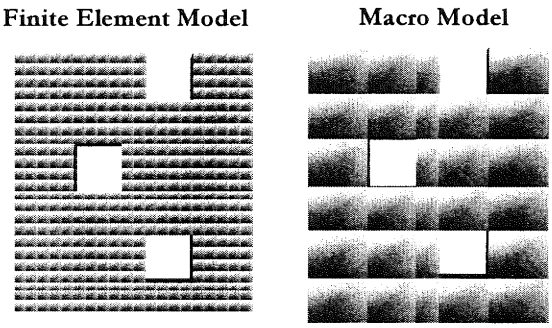

Figure 1. Modelling Grids

As noted above, the macro elements used are a combination of elements intended to represent either or both the shear and flexural modes or response. The development of element rules for each type of response is described in the following sections.

3. SHEAR CONTROLLED WALLS

Shear controlled walls are those in which the shear strength of the wall is lower than the flexural strength. These walls are characterised by relatively low ductility, as shown by the hysteresis shown in Figure 2, extracted from Reference [7]. This curve is typical of the experimental data on this type of wall.

The force-displacement relationship for this type of wall is a complex interaction of flexure, diagonal cracking, sliding shear, starter pullout and other factors. Attempts to explicitly model these characteristics have not been successful and so an empirical approach was adopted for this development.

The empirical hysteretic model for shear controlled walls was developed from experimental data on squat shear walls, code requirements [5] and recommendations in the FEMA guidelines for the evaluation of shear wall structures [8].

The backbone curve developed from these sources has the characteristics shown in Figure 3. The initial elastic stiffness (Line 1 on Figure 3) is based on code definitions of the shear modulus for concrete. The peak of the curve is anchored at the FEMA recommendation of the concrete strength plus expected steel strength (1.25 times the nominal strength) at a drift ratio of 0.0075 (End of Line 3 in Figure 3). FEMA guidelines also defined the residual strength, Line 5 in Figure 3. Between these limits, intermediate points were added to match the general shape of the experimental data.

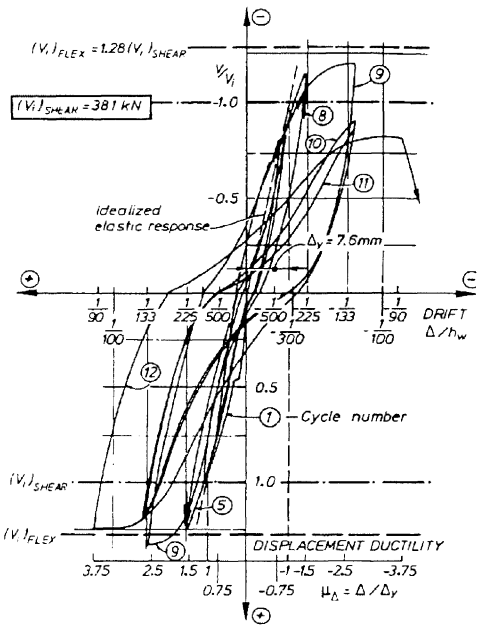

Figure 2. Test Hysteresis

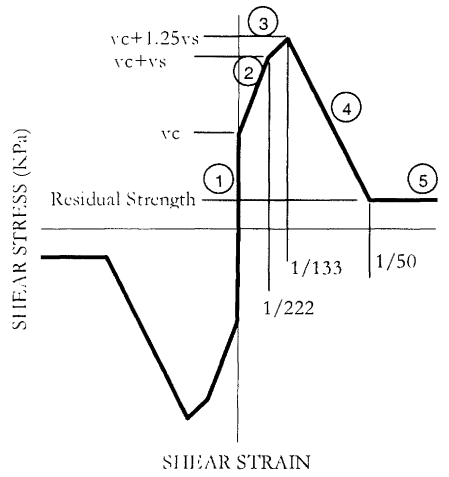

Figure 3. Backbone Curve

The backbone curve as implemented is defined by five branches:

1. Elastic Stiffness. An initial linear elastic stiffness applies for stress levels up to the calculated shear strength of the concrete alone, v_C. The shear modulus, G_0, is based on the formulations for the elastic modulus and Poisson's ratio of the material, defined in codes such as NZS3101 [5].

2. Cracked Stiffness. For stresses exceeding v_C, a reduced tangent shear modulus is calculated as in Equation (1), using v_S, the shear strength provided by the steel, and γ_C, the shear strain at which the concrete shear strength, v_C, is reached. The shear strain of 0.0045 was selected as an intermediate point, at which test results indicate that the stiffness reduces.

$$G_1 = \frac{v_S}{0.0045 - \gamma_c} \quad (1)$$

3. Strain Hardening. A combined overstrength and strain hardening factor of 1.25 (defined as expected strength in FEMA) is applied to v_S and the tangent modulus of the third branch of the backbone curve is defined as in Equation (2):

$$G_2 = \frac{0.25 v_s}{0.0075 - 0.0045} \quad (2)$$

4. Strength Degradation. For shear strains exceeding the strain at peak strength of 0.0075 the strength degrades to a residual strength level at a strain of 2.67 times the strain at peak strength, or 0.020.

5. Residual Strength. A plateau at the residual strength for strains exceeding 0.020.

These limits match those specified by FEMA 356 [8] for shear wall components where the response is dominated by shear, which specifies a drift ratio of 0.75% (1/133) for peak strength and the limiting drift at 2% (1/50). Based on FEMA tables, the residual strength ranges from 0.20 to 0.60 of the peak strength, depending on the component.

The unloading characteristics are defined by two parameters, α, which defines the strain limit, and β, which defines the stress limit, as shown in Figure 4.

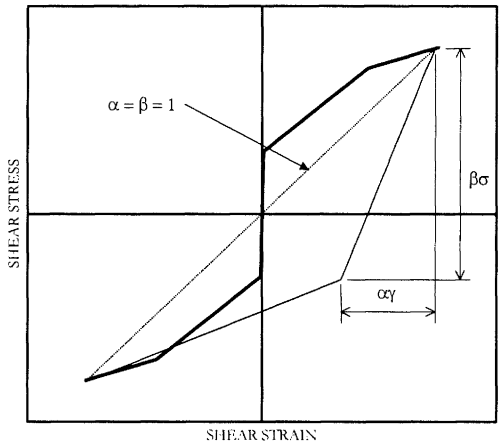

Figure 4. Unloading Characteristics

If both $\alpha = \beta = 1.0$ then unloading is along the secant stiffness through the origin. This is appropriate for brittle materials such as unreinforced masonry but for ductile materials such as reinforced concrete values are typically $\alpha = 0.5$ and $\beta = 1.0$, to produce the hysteresis shown in Figure 5.

The values of α and β are empirical, selected to match the approximate hysteresis area indicated from experimental data.

The backbone curve defines the points at which the element properties change, and with the unloading factors define the hysteretic curve shown in Figure 5. On a loading cycle, the

tangent shear stiffness reduces to zero once the loading curve intersects the backbone curve. The strength is maintained until the element unloads, after which it follows the unloading path defined by α and β.

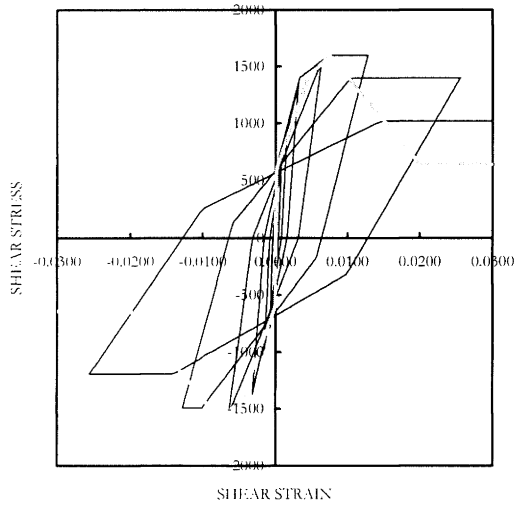

Figure 5. Shear Hysteresis Function

3 FLEXURAL WALLS

For a cantilever shear wall, the flexural mode of performance is more deterministic than the shear mode as the resistance is provided by a relatively simple couple formed by the reinforcing in tension and the concrete in compression. Figure 6 shows a typical hysteresis curve for a ductile shear wall, extracted from FEMA 307 [9]. Although the mechanism for flexure is well defined, the shape of the hysteresis loop is complex. This is because of the effects of shear cracking and axial load on the specimen.

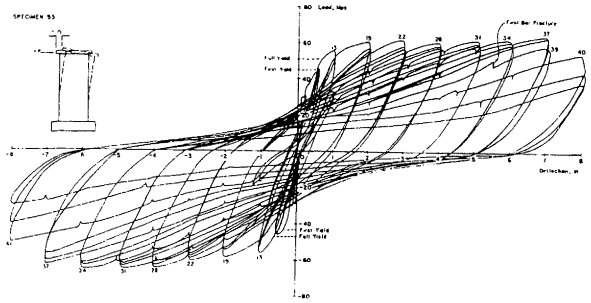

Figure 6. Flexural Wall (FEMA 307, from Corley et al).

The basic mechanism of a cantilever wall can be examined using an engineering mechanics approach for a section with flexural steel lumped at each end, as shown in Figure 7.

An applied lateral load, V, will be resisted by two components, the applied axial load, P, and the tension force in the reinforcing at each end of the wall. The peak resistance can be calculated by taking moments about the toe of the wall.

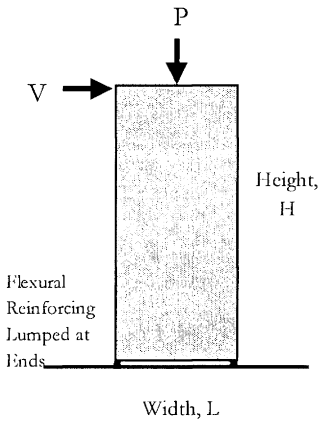

Figure 7. Wall Configuration

Ignoring vertical load, the shear force required to cause tension yield in the reinforcing at one end of the wall, V_B, is:

$$V_B = \frac{A_s f_y L}{H} \tag{3}$$

where A_s is the steel area at one end and f_y is the steel strength. Under reversing loads the steel couple produces a stable hysteresis loop, as shown in Figure 8 (a).

Assuming the tension capacity of the concrete is zero, the resistance supplied by the axial load at a lateral displacement Δ is:

$$V_P = \frac{P}{H}\left(\frac{L}{2} - \Delta\right) \tag{4}$$

For most cantilever shear walls the displacement, Δ, is small compared to the wall length and so the slope is close to horizontal. Unlike the steel couple, the axial load alone does not produce a hysteresis curve but unloads elastically. On unloading the force follows the same path as for loading, as shown in Figure 8 (b).

The summation of these two curves, one hysteretic and the second elastic unloading, produces the combined shape shown on Figure 8 (c). This type of hysteresis, which is generally termed *pinched* or *waisted*, is a characteristic of reinforced concrete elements under combined moment and axial load, which includes columns as well as walls.

In practice, the hysteresis shape is more curved than shown in Figure 8 (c) because of the effects of concrete stress block size, distributed reinforcing, shear cracking, the Bauschinger effect and contact stress effects in the concrete. The pinching effect tends to reduce the energy dissipation capacity of this type of section as the axial stress increases.

Figure 9 shows the interaction diagram generated for a 500 mm wall, 25m high x 5 m long. Also shown on the plot are the hysteresis shapes at axial load levels of 0, 2000, 5000 and 10,000 kN (0, 0.027, 0.067, 0.133 f'_c). These axial load levels are below the balanced load and yet the hysteresis shows extreme pinching at the higher load levels. In practice, most shear walls have axial stresses less than $0.05f'_c$ and so the pinching is unlikely to be as extreme as shown in Cases 3 and 4 in Figure 9.

Some innovative forms of construction currently being developed use post-tensioning to increase vertical stress on the wall to increase the restoring force and avoid damage. The additional load imposed in this form of construction produces the characteristics *flag* shaped hysteresis shown at the highest axial load level in Figure 9.

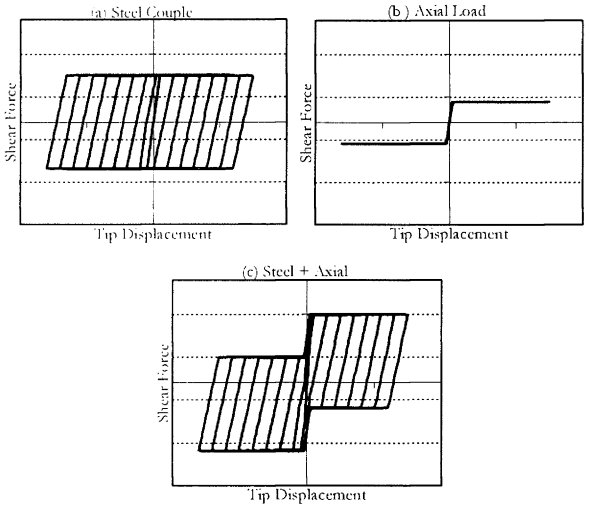

Figure 8. Cyclic Force-Displacement Function

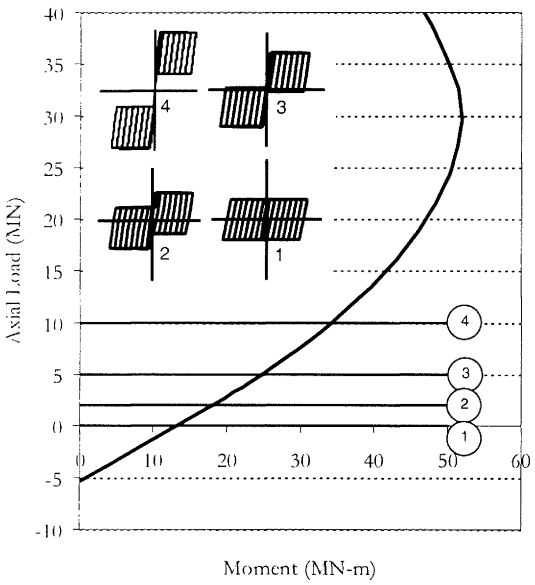

Figure 9. Interaction Diagrams for Wall

4 IMPLEMENTATION OF SHEAR WALL MODEL

For implementation of the shear wall model, a flexural model at the base of the wall was added to the empirical model for the shear controlled wall.

As the shear model includes some component of flexural deformation, adding a flexural model may overestimate total flexural deformations. However, the design philosophy for flexural walls is to provide sufficient shear steel to resist the shear forces generated by overstrength plastic hinging at the base of the wall. This design procedure restricts shear stresses to less than $v_c + v_s$, and so the shear response will be restricted to Lines 1 and 2 in Figure 3. In this case, flexural deformations will dominate.

4.1 Computer Software

The shear and flexural modes of response were implemented in the *ANSR-II* computer program [10]. This is a general purpose nonlinear analysis program developed at the University of California, Berkeley.

The original program included truss and gap elements which were suitable for modelling the flexural mode of response. The program also included a nonlinear two-dimensional plane stress element but the material model for this element was elastic-perfectly plastic with Von Mises yield criteria. This element was modified so that yielding was a function of total shear strain, with limits based on a piece-wise linear backbone curve as described earlier in Figure 3. Rules were coded to follow the loading / unloading paths shown in Figure 5. The model was originally developed for reinforced masonry [11] and was extended for concrete walls by modifying the unloading options. It has been shown to be capable of capturing the overall characteristics of shear wall structures [12].

For implementation the geometry of the structure, material properties and details of the walls and other structural elements are entered on a spreadsheet. A pre-processor program then assembles this data into the input format for *ANSR-II*.

4.2 Example Wall

The development procedure for a concrete shear wall analysis model is illustrated with an example wall, as shown in Figure 10. This is a 500 mm thick wall, 25 m high x 5 m wide wall. The reinforcing ratio is 0.5% with the steel distributed evenly across the section.

Note that the grid used in this example is suited for single component models and is more refined than the macro models typically used for full building analyses. The effect of grid size on results is examined in more detail later in this paper.

4.3 Flexural Yielding

Flexural yielding was modelled using pairs of elements at each node point across the base. A compression-only gap element represented the concrete stress block and a bi-linear truss element represented the reinforcing. Each pair of elements together provide the non-symmetrical force-deformation properties shown in Figure 10.

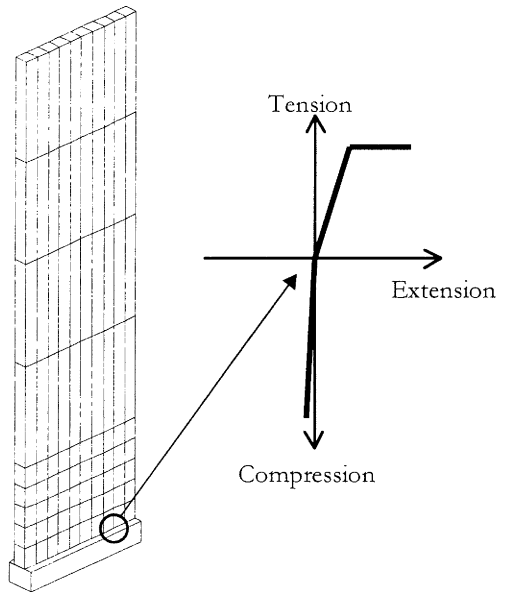

Figure 10. Analysis Model

The elements have axial stiffness only with the stiffness defined as K = EA/L. The elastic modulus, E, is known for steel and concrete and the area of each material, A, can be calculated from the wall dimensions and reinforcing content based on the area tributary to each node.

This type of flexural model essentially assumes a single, horizontal flexural crack across the base of the wall. This is a very simplistic approach as diagonal cracking causes tension lag which increases flexural deformation and also the effective stiffness is a function of tension stiffening, where the wall remains elastic between flexural cracks. In the model, these effects are incorporated by adjusting the length of the tension element, L, so that it represents the integration of the length of bar which is subjected to yield strain.

Comparison with experimental results has suggested that an effective length of approximately $10d_b$, where d_b is the diameter of the flexural reinforcing, provides a reasonable estimate of the ultimate capacity. This length may be interpreted as the equivalent yielding length of reinforcing. As yield is assumed over the full element length in the model, it could be expected that this length would correlate to about one-half the development length.

For most full size structures a yield length of 250 mm is satisfactory. For the small scale test specimens with small diameter bars, as described later in this paper, a shorter length is appropriate.

In a discussion to Reference [13], Priestley & Paulay quote experimental evidence that the effective strain penetration length, over which strain may be considered equal to yield, is $4400\varepsilon_y d_b$, in both directions (up into the wall and down into the foundation). This corresponds to $13.2d_b$ for f_y = 300 MPa and $18.9d_b$ for f_y = 430 MPa. This suggests that the value of $10d_b$ may be a lower bound value. However, presumably the effective strain penetration length from Reference [13] is the maximum value, applying to bars at the wall edges. It seems reasonable that an average value to apply to all bars would be lower than this maximum value.

4.4 Strength and Stiffness

The shear stiffness, as defined in the backbone curve in Figure 3, requires an initial shear modulus, G, and the shear strength of the concrete and steel respectively, v_C and v_S.

The initial shear modulus is calculated using NZS3101 formulations for elastic modulus $E_C = 3320\sqrt{f'_C} + 6900$ MPa and Poisson's ratio $\nu = 0.2$ as:

$$G = \frac{E_c}{2(1+\nu)} \qquad (5)$$

The concrete shear stress, v_C, is calculated using the NZS3101 maximum allowable shear $v_C = 0.2\sqrt{f'_C}$, which for 30 MPa concrete allows 1.095 MPa.

The shear strength provided by the reinforcing is calculated as $v_S = p_H f_Y$ where p_H is the horizontal steel content and f_Y is the yield strength of the steel.

The flexural strength and stiffness is defined by the truss and gap elements representing respectively the concrete and steel. The concrete stiffness is calculated using E_C, the area of wall tributary to the node, Ac, and an effective joint width (gap length) of 250 mm. The concrete is assumed linear elastic. The steel truss stiffness is calculated using E_S and the area tributary to the node, calculated as $A_C p_V$ where p_V is the vertical steel content, assumed 0.5%.

4.5 Lateral Loading

The lateral stiffness of the model was determined by applying an increasing displacement to the top of the wall and recording the force required to produce each displacement increment. The force-displacement function obtained is as shown in Figure 11, for the case with zero axial load.

As the wall displacement increases the truss elements representing the reinforcing progressively yield in tension and the points at which this occur are marked on Figure 11. A maximum of 9 of the 11 truss elements yielded in tension, with the other two truss elements remaining within the concrete stress block.

Also plotted on Figure 11 is the theoretical load curve, based on the moment capacity as calculated from an interaction diagram. The theoretical displacement at yield is based on the NZS3101 [5] Commentary factors of 0.25 on flexural stiffness (I_G) and 0.50 on shear stiffness (A_G). These are extracted from Table C3.1, for walls with $N^* = 0$.

There has been much discussion regarding appropriate stiffness values to use for flexural walls (References [13,14]). These discussions relate to an effective stiffness suitable for seismic analysis, such as the 0.25 factor from NZS3101.

From Figure 11, it is seen that the effective stiffness from the model depends on the point selected to define the secant curve. The stiffness is essentially linear, equivalent to $0.70I_G$ up to the point where 5 bars across the section have reached yield, at a moment of $77\%M_u$. As successive bars yield the stiffness reduces. At the point where 8 bars have reached yield $M = 90\%M_u$ and $I_{EFF} = 0.26I_G$. The ultimate

moment is reached when 9 of the bars yield (the other two are within the compression block) and at this stage $I_{EFF} = 0.11I_G$.

The curve shown in Figure 11 illustrates the difficulty in defining a yield displacement for a shear wall section. Calculation of the ultimate moment assumes that all tension steel reaches yield strain based on a plane section formulation. For tension bars close to the neutral axis this can imply an extremely high curvature on the section. The high yield curvatures are most pronounced for lightly reinforced walls with distributed reinforcing and C and L shaped walls, where the depth of the compression block is small.

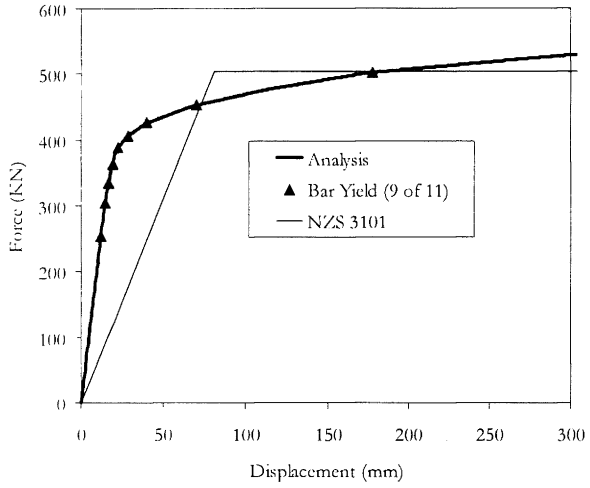

Figure 11. Loading Curve

4.6 Cyclic Loading

Under cyclic displacements applied at the top of the model, the deformed shape is as shown in Figure 12, with deformation dominated by rotation of the base wall plastic hinge.

At the tension side of the wall the gap elements separate and the truss elements yield in tension. On the compression side of the wall the majority of the load is resisted by the gap element with the remainder resisted by the truss element in compression.

When the wall rocks high shear stresses arise in the plane stress elements adjacent to the compression zone. These shear stresses cause the lower, outer elements to crack and eventually degrade. Elements in which the strength has degraded are indicated with an X in Figure 12. Elements which have cracked but in which the stress has not exceeded the ultimate stress are marked with a / or \.

Figure 12. Wall Cracking

4.7 Concrete Shear Strength

When using code requirements for the design of concrete shear walls, the shear strength provided by the concrete in the plastic hinge zone is reduced to that provided by friction due to axial load only and the total allowable nominal shear stress is reduced as the ductility demand increases.

Code design assumes an average shear stress across the wall section. Under cyclic loading, the edge finite elements under the concentrated compression elements are subject to higher shear stresses than the elements on the tension side of the wall. This results in local shear strains such that the strength of the panel degrades. As shown in Figure 12, under cyclic load a permanent strength loss occurs on both sides of the wall.

This process progressively implements the loss of concrete shear strength as the ductility demand on the wall increases. Therefore, the initial conditions for the analysis assume the code concrete strength. The actual concrete contribution to total shear strength reduces as the strain in elements exceed the shear strain at which strength loss initiates.

4.8 Hysteresis Curves

The model was used to generate hysteresis curves for four levels of axial stress, as shown in Figure 13. The horizontal lines on these plots are the theoretical strength, calculated as the moment strength from the interaction diagram divided by the wall height. The prototype wall is 25m high and so the peak displacement of 1000 mm shown on the plots corresponds to a wall drift of 4.0%.

The hysteresis curves in Figure 13 exhibit the pinching effect expected from engineering mechanics but the curves are more irregular due to the effects of distributed reinforcing, which causes progressive yield, and the shear cracking and degradation.

The peak capacity from the analysis exceeds the theoretical capacity by from 5% to 20%. Some moment increase is expected as the steel strain hardens, so as to reach a strength of $1.25f_y$ at the maximum displacements. The peak capacity generally occurs at drifts levels of 2% to 3% and then reduces as the applied displacement increases. This is

because of strength loss of the concrete at the extreme fibres and consequent reduction in effective lever arm. This strength loss does not occur in the example with no axial load as shear stresses in the extreme fibres are lower.

The walls with low axial load show a characteristic plateau on reloading after a large amplitude positive or negative displacement. This is most pronounced for the zero load wall and becomes less distinct as the axial load increases. This plateau represents the strength of the reinforcing alone as no concrete is in compression until the displacement is sufficient to close the gap opened by tension steel yielding. Higher axial loads act to close this gap earlier on load reversal.

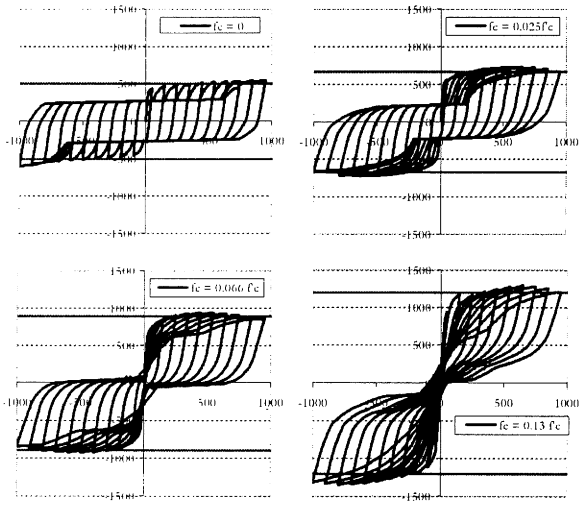

Figure 13. Force-Displacement Curves

5 COMPARISON WITH EXPERIMENT

The model development described in the previous section has demonstrated that this form of shear wall model is capable of capturing aspects of hysteretic response expected from engineering mechanics and experimental evidence.

For the next stage in the development, numerical results predicted from the model were compared with experimental values from test programs on a solid rectangular wall, a solid tee-shaped wall and a series of perforated walls.

5.1 Solid Wall

The solid wall used was part of a series reported by Paulay and Goodsir [15]. Wall 2 of this series was rectangular in section with dimensions of 1500 mm long by 100 mm thick. The wall was 2400 mm high. The wall section was symmetric, with confined cores acting as boundary members at each end of the wall.

Although the section was symmetric, an eccentric varying axial load was applied, resulting in non-symmetric response. The position of this eccentric load, plus the presence of confined boundary members, defined the finite element grid shown in Figure 14. Internal nodes across the section and up the height of the section were selected to provide reasonable aspect ratios for the elements, preferably not exceeding 2:1.

Element properties were defined as listed in Table 1, based on the details provided in Reference [15]. The concrete shear strength was based on $v_C = 0.2\sqrt{f'_C}$ throughout the wall. The effective length of the flexural elements was set as 120 mm, based on 10 times the maximum bar size of 12 mm.

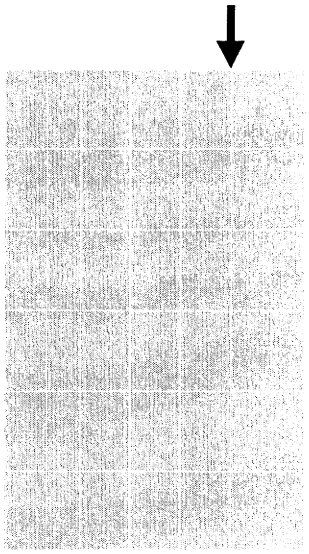

Figure 14. Model of Wall 2

Table 1. Wall 2 Model Properties

	p_V	v_C (MPa)	v_S (MPa)	T (mm)
Ends	0.0471	1.095	3.857	100
Centre	0.0032	1.095	2.059	100

The loads applied to the model duplicated those in the test, an applied lateral displacement increasing with each cycle and a concurrent axial load, varying sinusoidally from 593.5 kN at the maximum positive displacement to 144.5 kN at the maximum negative displacement.

For low amplitude displacements, damage was restricted to gap opening and yielding of the flexural reinforcing at the base, as shown in Figure 15.

As the amplitude of the applied displacements increased, shear damage occurred in the panels. The damage was concentrated across the base and in vertical strips adjacent to the confined boundary members, as shown in Figure 16.

The shear degradation at high displacements results in vertical dislocations of the panels so that the plane section at the plastic hinge no longer remains plane, as shown in Figure 16. This resulted in a loss of strength.

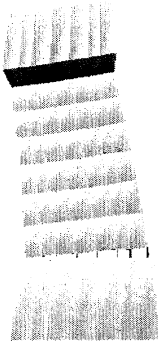

Figure 15. Yielding in Early Cycles

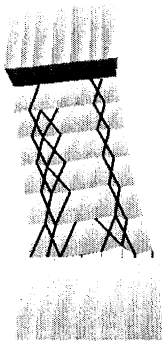

Figure 16. Damage at Last Cycle

Figure 17 plots the hysteresis curve obtained from the analysis. The output from the analysis included the applied displacement and the force at the top of the wall required to cause this displacement, F. The base moment at the wall centroid was then calculated at each displacement increment as:

$$M = Fh + Pe \qquad (6)$$

where h was the wall height (2.400 m), and e the eccentricity of the vertical load, P (0.375 m).

The ideal moment capacity and the maximum moments from the test and the analysis are listed in Table 2.

Table 2. Wall 2 Results

	Positive Direction	Negative Direction
Ideal Moment, M_i	1057	-839
Maximum from Test	1286	-997
Maximum from Analysis	1150	-944
Analysis / Test	0.89	0.95

The peak analysis moments exceeded the ideal moment capacity, as did the experimental moments, because of steel strain hardening. Maximum moments from the analysis were 11% and 5% lower than the experimental results for positive and negative directions of loading respectively.

Figure 18 is a reproduction of the hysteresis obtained from the test. In general, the analysis produces a similar strength at similar levels of displacement to those measured. However, in the test the ultimate failure for displacements exceeding 70 mm was a sudden buckling failure, a mode not included in the model. Therefore, the strength loss was not as dramatic in the analysis as it was in the test.

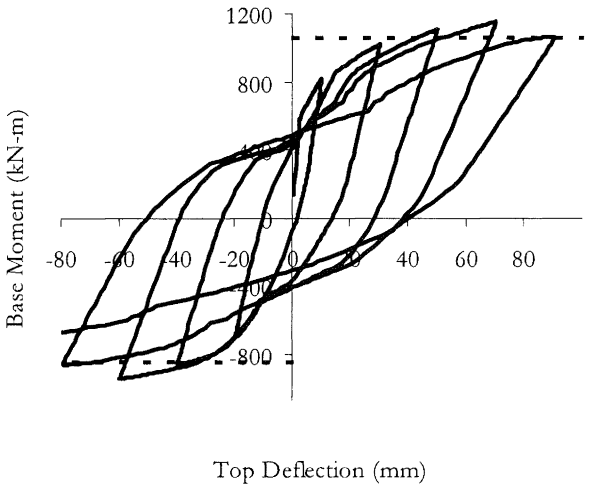

Figure 17. Wall 2 Analysis Hysteresis

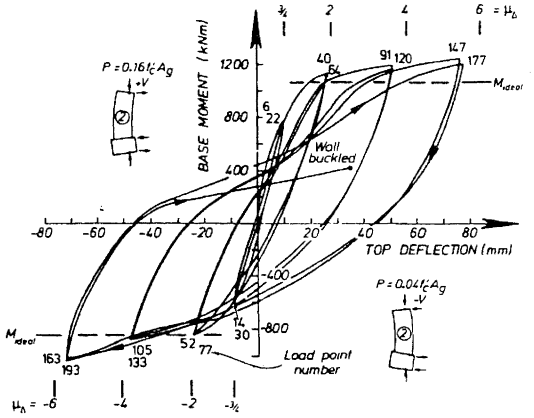

Figure 18. Wall 2 Test Hysteresis

5.2 Tee-Shaped Wall

Wall 5 of the Paulay and Goodsir series [15] was a tee-shaped wall, also with an eccentrically located, varying axial load. A model was developed using the same principles as for Wall 2, with the grid layout defined by the requirement to locate the confined boundary regions at the end of the walls and the axial load location (Figure 19).

Also as for Wall 2, material properties were based on a concrete shear strength of $v_C = 0.2\sqrt{f'_C}$ throughout the wall and steel shear strength and flexural strength based on the horizontal and vertical reinforcing ratios respectively. Table 3 summarises the properties used for the model.

Table 3. Wall 3 Model Properties

	p_v	v_c (MPa)	v_s (MPa)	T (mm)
Web End	0.0240	1.095	5.890	100
Web	0.0031	1.095	2.166	100
Flange Ends	0.0389	1.095	3.686	100
Flange	0.0049	1.095	1.216	100

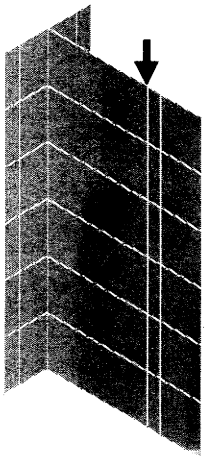

Figure 19. Model of Wall 5

Under increasing lateral load, flexural yield occurred in both the flange and web of the wall. As the amplitude of the displacements increased shear cracking and degradation occurred up the height of the wall in the lightly reinforced regions adjacent to the confined boundary. Figure 20 shows the damage pattern in the final cycle.

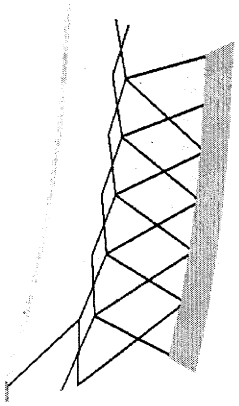

Figure 20. Damage to Wall 5

Table 4 compares the ideal moments with the peak moments recorded in the tests and the analysis. As for Wall 2, strain hardening increased the capacity beyond the ideal value. The peak analysis moments were 4% higher than the test moments in the positive direction and 5% lower in the negative direction of loading.

Table 4. Wall 5 Results

	Positive Direction	Negative Direction
Ideal Moment, M_I	980	-584
Maximum from Test	1218	-883
Maximum from Analysis	1267	-839
Analysis / Test	1.04	0.95

Figure 21 plots the analysis hysteresis for the same sequence of loading as the experimental wall, which produced the hysteresis shown in Figure 22. For both analysis and test the wall failed after cyclic displacements exceeding 100 mm. Test failure was due to concrete crushing, analysis failure due to degradation of shear strength.

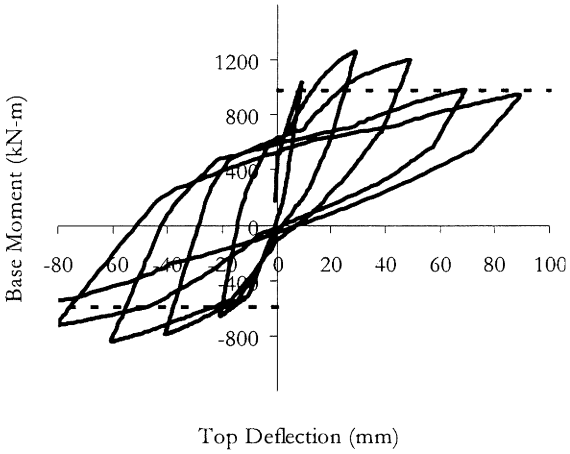

Figure 21. Wall 3 Analysis Hysteresis

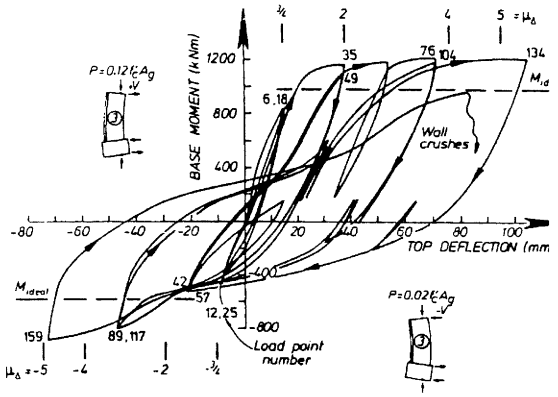

Figure 22. Wall 3 Test Hysteresis

The analysis model is based on a total shear formulation, where the shear stress in the model arises from applied horizontal loads plus compressive forces caused by flexure. Therefore, although concrete crushing is not included explicitly in the model the increase in shear due to the

compression reaction may initiate failure as occurred in this example.

5.3 Perforated Walls

Yanez, Park and Paulay reported the results of a series of tests on six reinforced concrete walls tested under reversed cyclic displacements [16]. All walls were 2.0 m long by 2.30 m high. Wall S1 was a solid wall and Walls S2 to S6 had varying configurations of openings.

Figure 23 reproduces the details of wall S2, which had irregular openings.

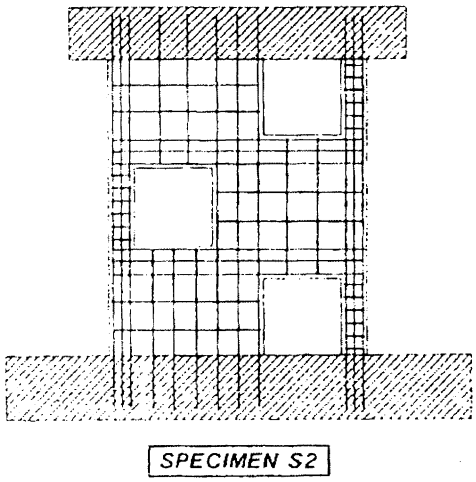

Figure 23. Test Specimen S2

For each of the six walls an analysis model was developed, generally based on the discretization required to locate all geometric features. Figure 24 shows the models of each wall.

All plane elements in the model were defined with a concrete shear strength of 0.96 MPa, based on $0.2\sqrt{f'_c}$, and a steel shear strength of 1.72 MPa, based on the horizontal steel content of 0.4% times a yield strength of 430 MPa.

Flexural yield was modelled with combined gap / truss elements. The area of the truss elements was based on the vertical steel reinforcing ratio, generally 0.50% but increased in end regions for walls with openings. Truss yield was based on a steel yield stress of 430 MPa. The effective length of the yielding reinforcing bars, which defined the gap width, was 80 mm, based on 10 times the flexural steel diameter of 8 mm.

Each model was analysed for an increasing displacement applied at the top of the wall, to approximately duplicate the loading regime used in the test.

For each wall, yielding occurred at the base of the wall and the concrete wall strength was exceeded in various panels of the wall, depending on the wall configuration. Figure 25 shows the damage to Wall S2. In this figure, a partial diagonal line indicates that the concrete shear strength is exceeded and a full length diagonal that the concrete plus steel shear strength is exceeded. For this wall, the shear stress in the right hand pier exceeded the shear strength and the element degraded.

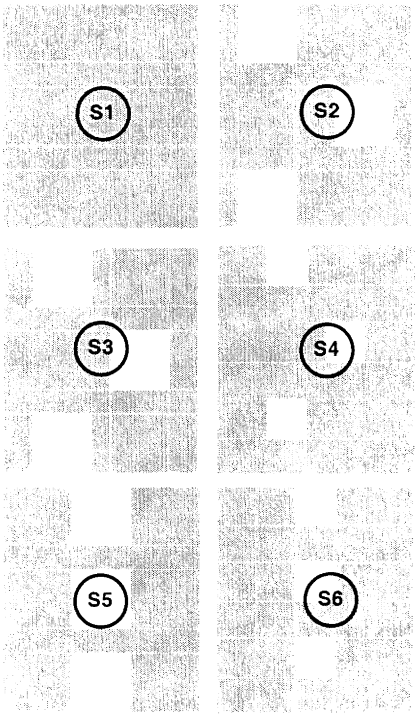

Figure 24. Wall Models

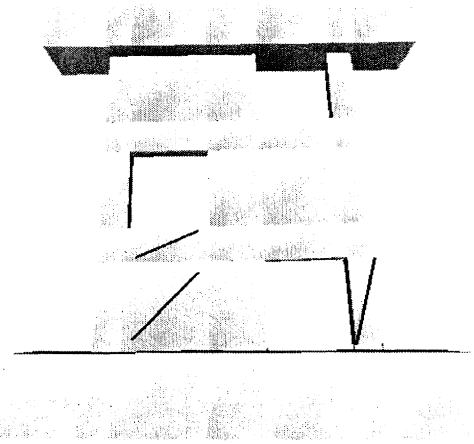

Figure 25. Damage to Wall S2

Figure 26 plots the analysis hysteresis for Wall 2, compared to the experimental hysteresis reproduced in Figure 27. The analysis hysteresis produces a similar level of strength to the experiment but differs somewhat in shape, particularly the reloading curves.

Table 5 compares the peak forces from the analysis with the experimental results for all six walls. Generally the analysis forces were within about 10% of the test results except for Wall S1, the wall without openings, where the analysis over-estimated the strength by 15%.

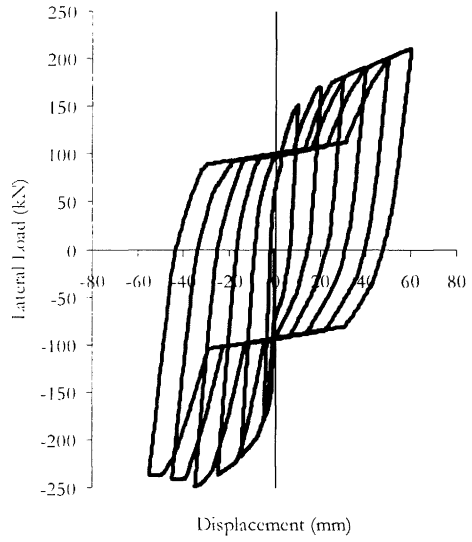

Figure 26. Analysis Hysteresis for Wall S2

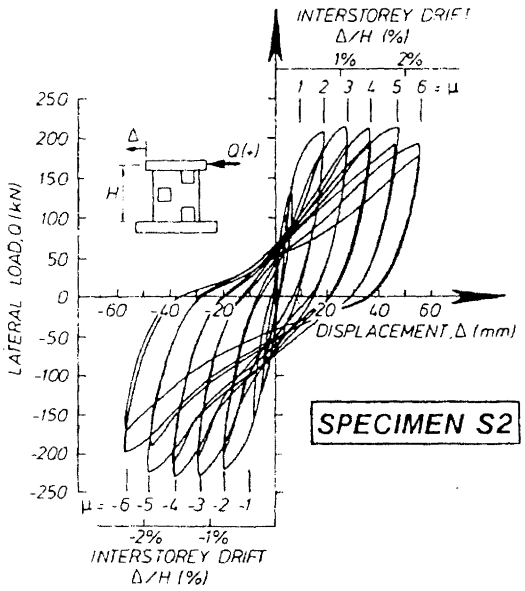

Figure 27. Test Hysteresis for Wall S2

Table 5. Wall Strength (kN)

	Analysis		Test		Analysis / Test	
Wall	V+	V-	V+	V-	V+	V-
S1	307	-300	287	-261	1.07	1.15
S2	211	-248	208	-228	1.01	1.09
S3	176	-221	217	-239	0.81	0.92
S4	223	-214	235	-236	0.95	0.91
S5	231	-226	233	-227	0.99	1.00
S6	255	-253	257	-246	0.99	1.03

The test program measured the stiffness of each wall, defined as the force at ductility factor 1.0. Figure 28 plots the experimental stiffness and compares this with the low displacement portion of the analysis hysteresis loop for Wall S2.

The model appears to have a higher initial stiffness than the test specimen. However, it is difficult to compare values directly as the experimental value of ductility factor 1.0 was related to the ideal strength of the wall. The applied displacements then related to this value. For the analysis, the displacement increment was set to 5 mm for all walls.

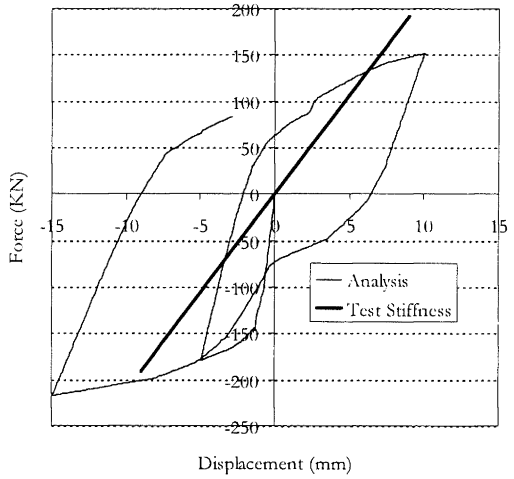

Figure 28. Wall S2 Stiffness

6 MODELLING PARAMETERS

6.1 Effect of Discretization on Strength

The model as developed is intended to be used with a coarse grid, often only a single element to represent the width of the wall. With such a representation, the uniformly distributed reinforcing steel is lumped in a truss element at each end of the wall.

Intuitively, it would appear that a section with half the reinforcing lumped at each end would have a higher moment capacity than the same area of reinforcing distributed across the section. However, the moment capacity will be the same in both cases for zero axial load. Consider the wall shown in Figure 29, with respectively 1, 2 and 3 elements.

Taking moments about the geometric centroid of the wall, for a single element,

$$M = \frac{L}{2}\left(\frac{T}{2}+\frac{T}{2}\right) = \frac{TL}{2} \qquad (7)$$

For two elements,

$$M = \frac{L}{2}\left(\frac{T}{4}+\frac{3T}{4}\right) = \frac{TL}{2} \qquad (8)$$

For three elements

$$M = \frac{L}{2}\left(\frac{T}{6}+\frac{5T}{6}\right)+\frac{L}{3}\left(\frac{T}{3}-\frac{T}{3}\right) = \frac{TL}{2} \qquad (9)$$

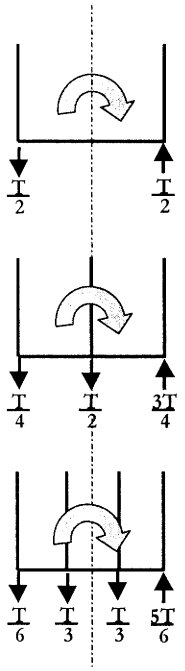

Figure 29. Calculated Moment Capacity

This suggests that the moment capacity will be the same for all configurations. This can be demonstrated by generating the interaction diagram for a shear wall section 4.000 m long x 250 mm thick with a flexural reinforcing content p_V = 0.5%, concrete strength f'_C = 30 MPa and steel strength f_Y = 280 MPa. Five discretization configurations are considered, as shown in Figure 30. In each case, the bar size is adjusted based on tributary width such that the reinforcing content is maintained at 0.5%.

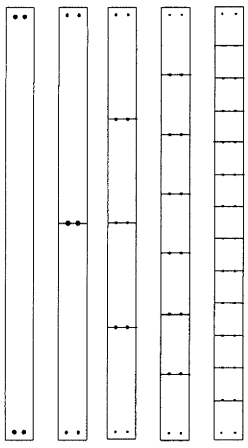

Figure 30. Discretization Configurations

Figure 31 plots the interaction diagrams generated for each of these five configurations. The first configuration, with all steel lumped at the two ends, produces a moment capacity higher than the other cases but the curves for the remaining four configurations are almost indistinguishable.

This is especially so for low levels of axial load, for example, as tabulated in Table 6 for an axial load of 2000 kN, which represents a stress of 2 MPa, close to the maximum usual axial stress for a shear wall. At this level of load the maximum error in moment capacity is 6% by modelling the wall as a single panel.

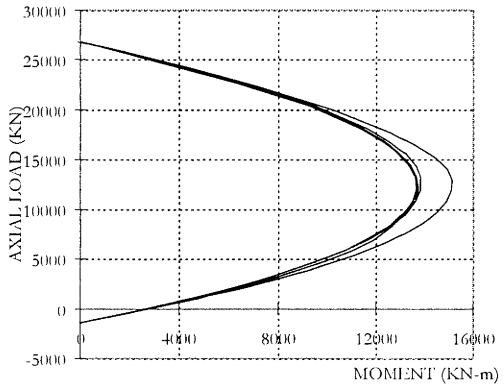

Figure 31. Interaction Diagrams

Table 6. Strength at 2 MPa Axial Load

Number of Elements	Nominal Strength M_U (kN-m)	Relative Strength
1	6368	1.00
2	6167	0.97
4	6040	0.95
7	5959	0.94
13	5954	0.94

Figure 32 shows the capacity curve generated for this wall at the axial load of 2000 kN for each number of elements tabulated in Table 6. This shows that the discretization has a minor effect on ultimate strength but a larger effect on the stiffness. With a single element there is a single yield event whereas for multiple elements there are multiple yield events, which provides for gradual yielding and a higher yield displacement.

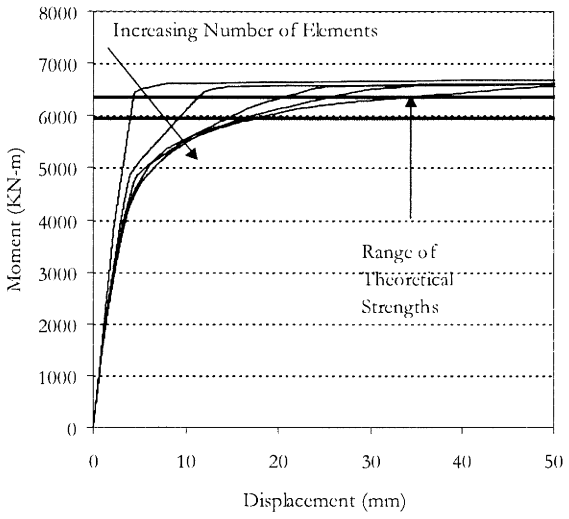

Figure 32. Analysis Strength

As the number of elements reduces the loading curve tends towards a bi-linear approximation, as is commonly used for other relationships, such as flexural element moment-rotation. This slightly over-estimates the area of the hysteresis loop but is accepted for nonlinear analysis.

6.2 Effective Joint Width

As the effective joint width (length of gap and bar elements) is increased the flexural stiffness of the section is reduced, as shown in Figure 33. These curves are all for the same steel content, p = 1%, and a strain hardening ratio of 0.005 in the steel. As discussed earlier, a joint width of 10 times the diameter of the flexural bars has been found to provide the best representation (the 250 mm width in Figure 33).

Figure 33 shows that smaller joint widths will produce a higher effective section strain hardening for the same steel strain hardening ratio. In practice, if the joint width is reduced the strain hardening ratio is also reduced to provide the correct level of strength increase.

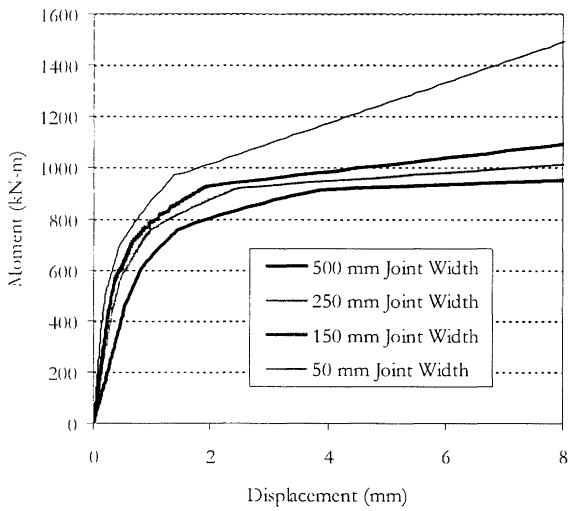

Figure 33. Effect of Joint Width

6.3 Steel Strain Hardening

The strain hardening ratio of the truss elements representing the reinforcing bars is defined as the ratio of the yielded stiffness to the elastic stiffness. As shown in Figure 34, this parameter has no effect on the initial stiffness of the wall but defines the amount of overstrength in the wall after yield.

The force-extension function applied to the truss defines the overall moment-deflection relationship in the wall section. As shown in Figure 34 and Table 7, this relationship is not quite linear. A strain hardening ratio of 0.1% produces an 8% overstrength at ductility factor of 5. If the ratio is increased to 1% the overstrength increases to 62%.

The strain hardening ratio is set so as to provide an overstrength appropriate to the material properties used to define the model. If nominal strengths were used then an overstrength of 1.25 to 1.35 would be appropriate. If material probable strengths were used then an overstrength of 1.10 to 1.20 would be more reasonable. From Table 7, for this particular wall a strain hardening ratio in the range of 0.002 to 0.005 would be appropriate.

Most building projects use a 250 mm effective joint width. For this width, a strain hardening ratio of 0.005 generally provides a reasonable moment-deflection relationship if nominal strengths are used to define element properties. A capacity curve can be used to quantify the moment overstrength and the ratio adjusted as required. The overstrength is also dependent upon the grade and source of the reinforcing steel.

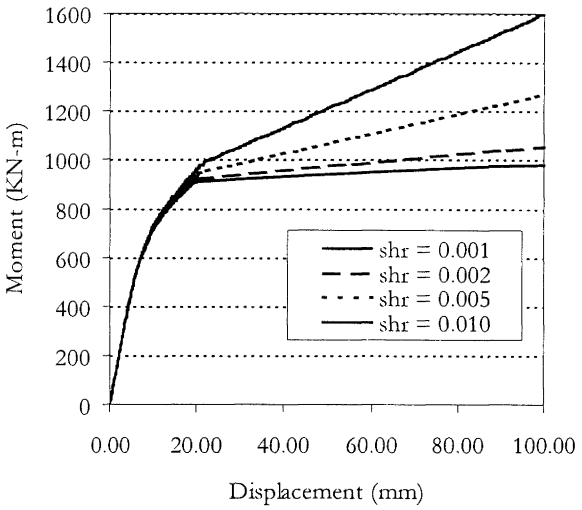

Figure 34. Effect of Strain Hardening Ratio

Table 7. Effect of Strain Hardening Ratio on Moments

Strain Hardening Ratio	Yield Moment M_Y	Ultimate Moment M_U at DF=5	M_U/M_Y
0.001	913	982	1.08
0.002	923	1055	1.14
0.005	943	1270	1.35
0.010	992	1604	1.62

7 EVALUATION OF PERFORMANCE

7.1 Shear Evaluation

The multi-linear model used to represent the shear mode of shear walls permits a direct evaluation of performance in that the shear strain is limited to the expected strength of the concrete plus reinforcing, which occurs at a shear strain level of 0.0075.

This limit corresponds to the FEMA-356 Collapse Prevention (CP) limit, which is a drift limit of 0.75% for wall segments of members controlled by shear.

For coupling beams the response is controlled by flexure and the shear strain is equivalent to the plastic rotation. FEMA-356 CP limits for these elements are in the range of 0.010 (high shear stress, conventional horizontal reinforcing, non-conforming transverse reinforcement) to 0.030 (diagonal reinforcement).

When walls are sub-divided, shear strain limits are applied to the story drift rather than to the shear strain in individual elements. This is because edge elements may have higher strains than internal elements due to combined horizontal and vertical shear (see Figure 12). The limits in sources such as FEMA-356 are based on the strain across the entire wall section rather than individual elements of the wall. For this reason, drifts are more appropriate than strain as an evaluation criteria.

7.2 Flexural Evaluation

Evaluation of the flexural performance of the wall is less straightforward than the shear evaluation because the flexural mode of behaviour is modelled using a number of elements.

FEMA-356 provides limits on the maximum plastic rotation for flexural walls as a function of axial stress, shear stress and the presence or otherwise of a confined boundary. CP limits range from 0.002 to 0.015 radians.

The plastic rotation, θ, can be calculated as $\theta = \delta / L_W$ where δ is the extension of the truss element at the edge of the wall and L_W is the length of wall in the model. This can be simply applied for straight walls but is more complex for shapes such as C and I, where the extension is a result of biaxial bending about both axes. Often, simplifying assumptions must be applied.

7.2.1 Low Cycle Fatigue

The reinforcing bars are explicitly modelled and the time history of plastic strain can be obtained from time history analysis. This leads to the possibility of developing flexural failure criteria based on low cycle fatigue. A procedure for this is outlined here. It has not yet been implemented and will be the subject of further study. However, it does appear promising as a method of explicitly defining the flexural failure point for a wall section.

The reinforcing bars deform plastically under seismic loading. For low-cycle fatigue, where a material is cycled at stresses exceeding yield, the fatigue behaviour under reversed cyclic loading is formulated in terms of the Coffin-Manson equation:

$$\varepsilon_p = \varepsilon_f (2N_f)^c \qquad (10)$$

where: ε_p = plastic strain amplitude
ε_f = a material constant to be determined from fatigue testing
$2N_f$ = number of complete cycles to failure
c = a material constant to be evaluated experimentally

For reinforcing steel, an experimental fit to this expression was obtained by Mander *et al.* [17]:

$$\varepsilon_p = 0.08(2N_f)^{-0.5} \qquad (11)$$

Figure 35 plots this function.

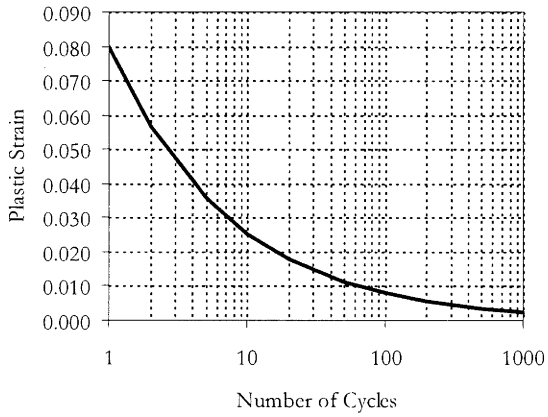

Figure 35. Low Cycle Fatigue Capacity

When a component is subjected to a number of cycles of different amplitude, Miner's linear cumulative damage rule is used:

$$\sum_{i=1}^{k} \frac{n_i}{N_i} \leq 1.0 \qquad (12)$$

To apply this formula, the ratio of the number of applied cycles to the number of cycles to failure at each particular strain level is calculated. The sum of these ratios is required to be less than 1.0.

Figure 36 shows the time history of plastic strain in Wall S1 of the Yanez series of tests [16] described earlier in this paper. This is used as an example of the application of low cycle fatigue theory.

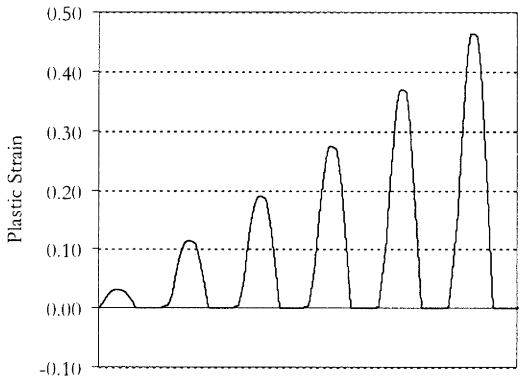

Figure 36. Reinforcing Strain for Yanez Wall S1.

The formulation of the Coffin-Manson equation in Figure 35 is based on full reversing cycles, from zero to maximum positive plastic strain to an equivalent negative plastic strain and back to zero. For reinforcing bars the plastic strain is only a half cycle, from zero to maximum tensile plastic strain

and back to zero as shown in Figure 36. It is likely that the number of half cycles to failure is two times the number of reversing cycles to failure plotted above. As we have no experimental data for that type of loading the criteria conservatively use the failure limit for full reversing cycles.

Wall S1 was loaded with one cycle at ductility Factor (DF) 1.0 and then two cycles of each of DF ± 2.5, ± 3.75 and ± 5.0 before failure by fracture of the flexural bars.

Table 8 shows the calculations for Wall S1 using Miner's rule with this strain history. The strain in the truss element represents the integration of strain throughout the plastic hinge length. In Table 8, an assumed plastic hinge length was used to obtain an equivalent distributed strain, ε_p*. A goal seek routine was used to solve for L_P so as to obtain failure in the reinforcing bars, defined as a sum equal to unity. The calculated plastic hinge length, 0.493 m, is equivalent to approximately $0.25L_W$.

Table 8. Failure Criteria for Yanez Wall S1

Applied N Cycles	ε_p for Model Length 0.080	ε_p* for L_P 0.493 m	Cycles to Failure N_f	Applied/ Failure
1	0.02	0.00	606	0.00
2	0.11	0.02	20	0.10
2	0.19	0.03	7	0.30
2	0.27	0.04	3	0.60
Sum				1.00

A formula for the plastic hinge length, L_p, from Priestley [18] is the greater of:

$$L_p = 0.2L_w + 0.03h_n \quad (13a)$$

$$L_p = 0.054h_n + 0.022f_y d_b \quad (13b)$$

where L_w = length of wall, h_n = wall height and d_b and f_y are the diameter and yield stress of the vertical reinforcing. For this wall, equation (13a) governs and provides a plastic hinge length of 0.469 m.

It is undoubtedly coincidence that the calculated plastic hinge length of 0.493 m correlates so closely with the Priestley value of 0.469 m. However, this does suggest that low cycle fatigue provides a promising method for evaluating flexural cyclic capacity.

7.3 Other Failure Modes

The evaluation criteria described above assess the primary modes of response, which are shear strains (or drifts) and flexural plastic rotations. Limits on each of these provide a means of assessing whether response is satisfactory.

As shown in the test programs used for validating the procedure, there are a number of material failure modes which may contribute to shear or flexural failure. Flexural failure can occur due to wall buckling for thin walls, fracture of flexural bars or buckling of reinforcing. The shear mode of failure may be due to sliding shear, diagonal cracking or web crushing.

The analytical hysteresis and evaluation criteria are applied without regard to the actual behaviour mode. In general, the hysteresis shapes are similar regardless of mode of response, with the main differences being in the point at which strength degradation commences and the rate of degradation.

The degradation parameters of the element formulation used can be adjusted to account for variations in strength loss. However, currently there is insufficient information available and so the generic backbone curves described in FEMA-356 are used.

8 EXAMPLE SHEAR WALL BUILDING

As an example of the application of the nonlinear analysis procedure, the 10 story prototype building produced as an example of design to NZS3101 is used ("Red Book", [19]). This was designed as a fully ductile structure with ductility factors, μ, of approximately 5.

8.1 Structural Model

The model included the non-seismic frames as well as the concrete walls, as shown in Figure 37. In order to enable direct correlation with the design, the columns and beams were pinned so that they did not contribute to lateral load resistance. Typically, non-seismic frames are included in the model so that the total seismic weight is represented. This ensures that there is a correlation between weight and mass such that full P-Δ effects will be included.

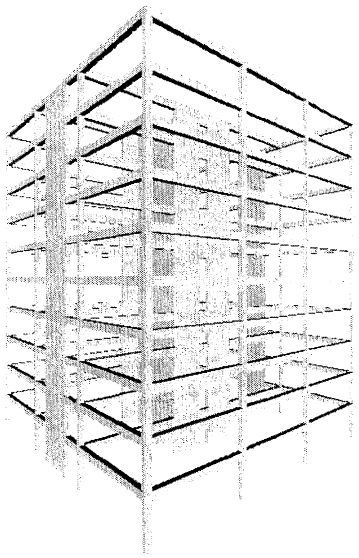

Figure 37. Full Model

Figure 38 shows the structural walls which form the lateral load resistance of the structure. In the X direction the walls are in the form of a C shaped wall (1) with two straight walls ((2 and 3) forming coupled walls with the flanges of the C wall.

In the Z direction, cantilever walls with boundary elements are placed at each end of the building (4 and 5). In this direction the C shaped wall also functions to resist lateral loads.

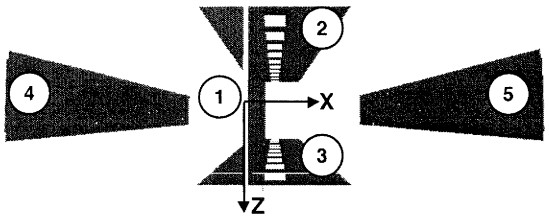

Figure 38. Wall Layout

The finite element discretization was sufficient to include geometric features of the wall (Figure 39). Each story was subdivided into two elements to enable the coupling beams to be modelled. The walls were modelled with one element horizontally, except where extra elements were required to define the coupling beams.

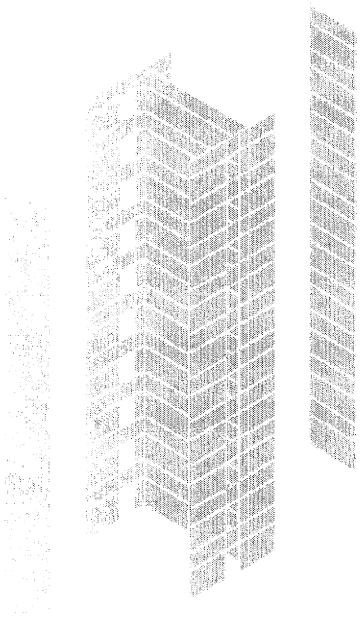

Figure 39. Finite Element Model of Walls

This finite element representation of the building has 1412 degrees-of-freedom, a relatively small model. This model takes about 7 minutes on a desktop computer for a single time history analysis (6000 steps at 0.005 seconds). For a singly symmetric building, an evaluation typically requires 18 analyses (3 earthquakes x 2 orientations x 3 centres of mass) so a full series can be run in about 2 hours. This turnover makes this type of analysis practical in a design office environment.

8.2 Element Properties

For all elements the concrete shear strength was defined as 1.095 MPa, based on the design concrete strength of 30 MPa. The shear strength provided by the steel was calculated from the design horizontal steel content and ranged from 1.7 MPa to 3.8 MPa for the walls.

The coupling beams were modelled as shear elements with a steel strength based on the design shear strength of the beam divided by the wall shear area. This provided steel shear strengths ranging from 1.7 MPa at the lower levels to 0.3 MPa at the upper levels. The hysteresis for the coupling beams was defined as stiffness degrading but with no strength degradation. This is achieved by setting the residual strength ratio to 1.0 and results in an elastic-perfectly plastic backbone curve.

Flexural yielding was included by pairs of gap/truss elements at each wall node at the base of the structure. The properties of each pair of element were calculated from the area of concrete and reinforcing tributary to the node.

The two end cantilever walls have columns functioning as boundary elements. These were included in the model as flexural elements sharing the same nodes as the ends of the panels representing the wall itself. The gap properties at the ends of the wall were adjusted by adding the concrete area of the column to the tributary wall area. Similarly, the area and strength of the parallel truss element were increased by the area of reinforcing in the column and the tensile strength of this reinforcing.

8.3 Dynamic Properties

Once a model was developed the periods and mode shapes were extracted to determine dynamic characteristics. The modal analysis was performed on a linear elastic model (panels uncracked, gaps closed) and so an effective stiffness of 0.35 times the gross stiffness was used in the panels, approximating the recommendations of NZS3101.

Table 9 lists the periods and effective mass factors for the first 9 modes. The first mode, with a period of 2.05 seconds, is X translation, the direction of the coupled walls. The 2nd mode has almost the same period, 2.00 seconds, and is torsional with a small Z translational component. This reflects the relatively low resistance to rotation provided by the wall configuration. The building is much stiffer in the Z direction, where the two straight walls plus the C-shaped wall provide a higher lateral stiffness. The 3rd mode is the fundamental mode in this direction, with a period of 1.06 seconds.

Table 9. Periods and Effective Mass

		Effective Mass			Cumulative Mass		
Mode	Period	X	Z	ROT	X	Z	ROT
1	2.050	64%	0%	0%	64%	0%	0%
2	1.997	0%	7%	59%	64%	7%	59%
3	1.064	0%	62%	8%	64%	70%	68%
4	0.407	0%	3%	19%	64%	73%	86%
5	0.400	23%	0%	0%	88%	73%	86%
6	0.267	0%	18%	3%	88%	91%	89%
7	0.173	0%	1%	6%	88%	92%	94%
8	0.170	6%	0%	0%	94%	92%	94%
9	0.127	0%	4%	1%	94%	96%	95%

8.4 Capacity Curve

The nonlinear capacity curve is generated by applying a static lateral load to the building and incrementing the load. The load pattern used was triangular, with maximum values at the top, corresponding to the equivalent static load pattern defined by codes. The load was applied in 1000 increments of 0.004W so that a total base shear of 0.4W would be applied. In practice, the analysis generally terminates once a mechanism forms and equilibrium cannot be achieved under increasing loads.

As the walls are non-symmetric, the loads were applied in both the positive and negative directions of the X and Z axes. The resulting capacity curves are plotted in Figure 40.

Figure 40 shows that the building is twice as strong in the Z (cantilever) direction than the X (coupled) direction. This is even though the design forces were only 25% higher (C_Z = 0.052 versus C_X = 0.042). The yield level of the building slightly exceeds the design strength in the X direction but is much higher in the Z direction because of the additional strength provided by the X walls acting as flanges when loads are in the Z direction. The capacity curve for the X direction differs for positive and negative directions of load whereas the Z curves is the same for both directions, reflecting the configuration of the walls.

To generate the capacity curves in Figure 40 the applied force is plotted against the displacement at the centre of mass, the point at which the lateral loads are applied. In the X direction the load resisting elements are symmetric and so the displacements are the same at all points on the floor. However, in the Z direction the centres of mass and stiffness do not coincide and so the translation is accompanied by a rotation. Figure 41 plots the capacity curve in the Z direction, as in Figure 40, and also plots the displacements at each end of the floor.

For centre of mass displacements of up to 200 mm the displacement at the East wall is effectively zero and the displacement at the West wall twice that at the centre of mass. This indicates that the torsional deformations are approximately equal to the translational deformations.

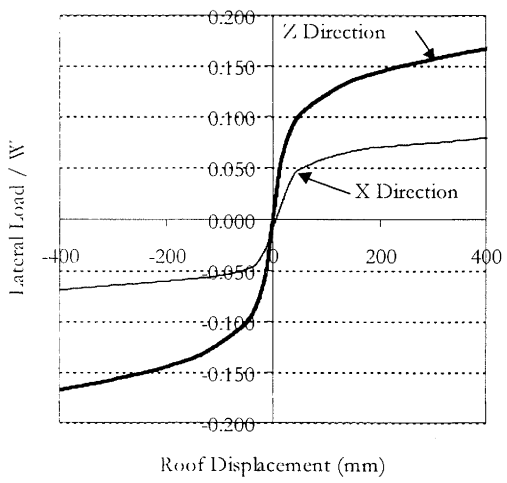

Figure 40. Capacity Curve

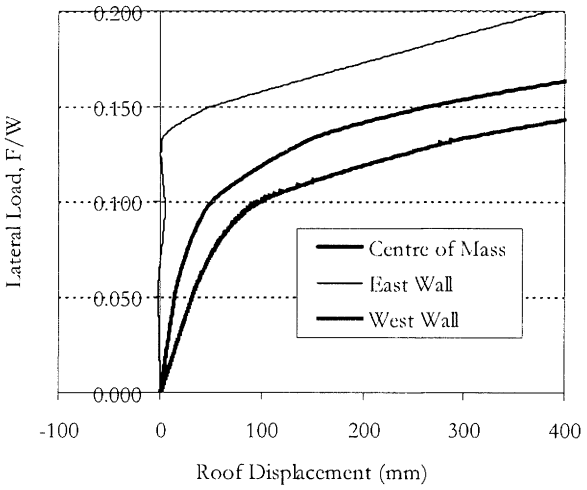

Figure 41. Z- Direction Displacements

8.5 Hysteresis

The capacity curve generates only the initial loading portion of the hysteresis. The full hysteresis can be generated by applying a cyclic displacement and recording the force required to produce this displacement.

In each direction the hysteresis was generated by applying an increasing cyclic displacement at the 7th floor, the floor closest to the effective point of application of the lateral load (2/3 height). The top floor displacement under this applied displacement is plotted in Figures 42 and 43 for the X and Z directions respectively.

The non-symmetry shows up very strongly in X direction, where the C wall provides part of resistance, whereas the Z curve is symmetric. In both directions the hysteresis loops are severely "pinched", with an area much less than would be produced by a bi-linear approximation.

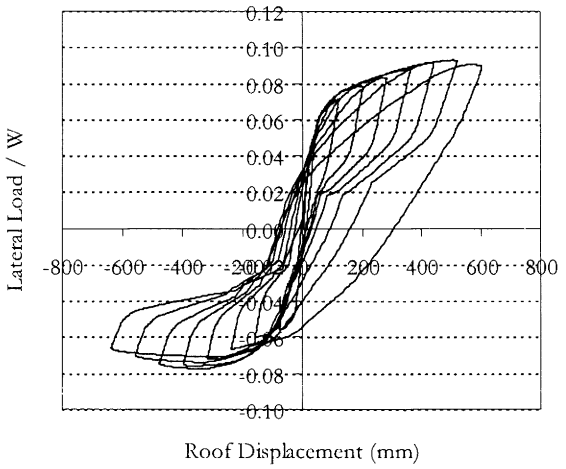

Figure 42. X- Direction Hysteresis

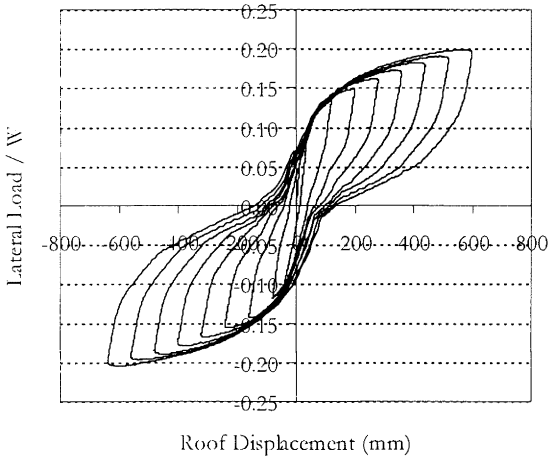

Figure 43. Z- Direction Hysteresis

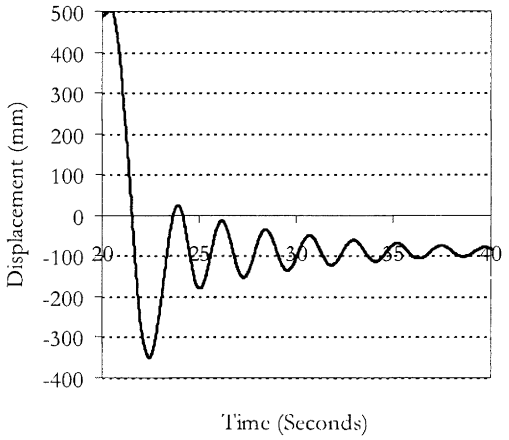

Figure 44. Decay Curve for X- Direction

8.6 Damping and Period

The periods, capacity curves and hysteresis curves provide a means of checking on the mass and stiffness properties of the model prior to performing a time history analysis. The other parameter which affects dynamic response is the damping in the structure. For most dynamic analyses damping is specified as Rayleigh damping, where the damping matrix, C, is formed as a combination of the mass matrix M, and the stiffness matrix, K, using:

$$[\mathbf{C}] = \alpha\,[\mathbf{M}] + \beta\,[\mathbf{K}] \qquad (14)$$

The constants α and β are referred to as the Rayleigh coefficients and can be calculated to define a specified fraction of critical damping at two periods. For periods between these two limits damping will be less than the specified value, for periods higher or lower the damping will exceed the specified value. The two periods are therefore selected to encompass the expected range of response of the structure.

For this building, damping was defined as 5% of critical for periods of 2.50 seconds and 0.05 seconds. An illustration of damping in the model can be provided by performing the analytical equivalent of a "snapback" test used to measure damping. A structure is forced into a deformed position, the restraint released and the free vibration of the structure measured. This provides an estimate of periodicity of response and, by measuring decay between successive cycles, the damping can also be extracted. Figure 44 shows the decay curve generated for this building in the X direction.

Figure 44 shows that, on release from a +500 mm top displacement, the building unloads to a displacement of approximately –350 mm and then cycles about an offset baseline. This offset is due to the non-recoverable cracking in the walls and plastic deformation in the base hinge.

The damping, ξ, between cycles n and n+m can be calculated from the peak displacements, Δ, using the formula for logarithmic decay:

$$\ln\frac{\Delta_n}{\Delta_{n+m}} = 2\pi m\xi \qquad (15)$$

To apply this formula peaks must be of the same sign and so a baseline correction is applied to the trace shown in Figure 44 by adding 89 mm to all displacement points. The period is then calculated as the interval between successive peaks of the same sign and the damping calculated at each cycle using Equation (15) with a value of m = 1. These are plotted in Figure 45.

For the initial unloading the period is long, 3.5 seconds, and the damping high, 25%. For subsequent lower amplitude cycles both the period and damping reduce and stabilise at values of 2.25 seconds and 5.2% respectively. The period of 2.25 seconds is about 10% longer than the period of 2.05 seconds calculated using effective stiffness. The damping of 5.2% is close to the target value of 5%.

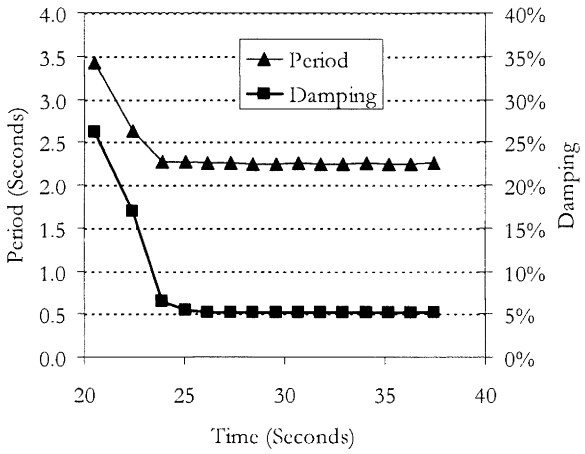

Figure 45. X- Direction Period & Damping

The logarithmic decay method is suited for symmetric structures, as in the X direction of this building, but less suited for non-symmetric structures, as shown in the decay curve in Figure 46 for the Z direction. There is very little displacement at the centre of mass but displacements of opposite sign at the two ends of the building. This indicates that the snapback test has activated the torsional mode rather than the translational mode.

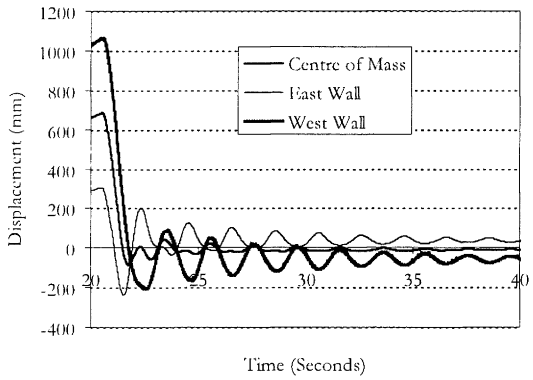

Figure 46. Decay Curve for Z- Direction

When the period and effective damping are extracted from the East wall decay shown in Figure 46 the functions shown in Figure 47 are obtained. The period of the first cycle is 3 seconds, reducing to an average of 1.93 seconds as the amplitude decreases. The damping similarly decreases from 30% to an average of 4.2%. The torsional period is slightly lower than the 2.00 second period from the elastic analysis, which indicates that the 0.35 effective stiffness factor was slightly lower than the effective analysis stiffness for this mode.

The damping of 4.2% is slightly less than the target value of 5% and this is because the period of 1.93 seconds is further from the upper limit of 2.50 seconds than the X period of 2.25 seconds.

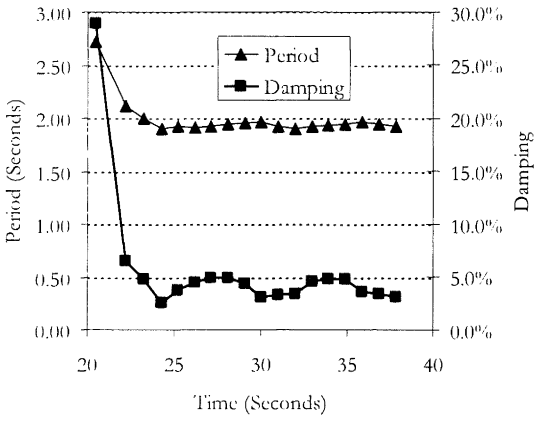

Figure 47. Z- Direction Period & Damping

8.7 Time History Analysis

8.7.1 NZS4203 Compatible

To enable a direct comparison with the design conditions, the initial time history analysis used a single time history applied along each axis of the building non-concurrently. The frequency content of the El Centro 1940 N-S component was adjusted so that the 5% damped response spectrum of the record was compatible with the NZS4203 [20] design spectrum, as shown in Figure 48.

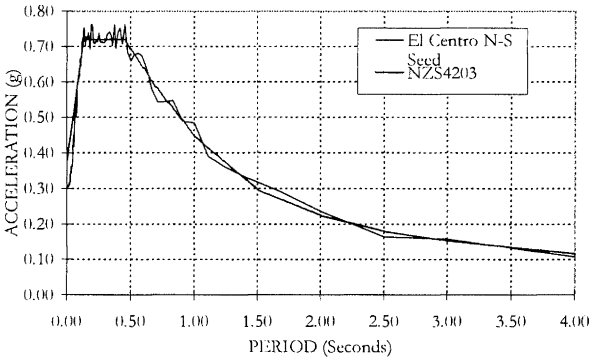

Figure 48. Spectrum Compatible Time History

The structure was analysed for the centre of mass location and for a ±0.1B eccentricity in each direction, a total of 6 analyses. As required by NZS4203 for time history analyses, the structural performance factor, S_p, was set to 1.0 so that the full amplitude of the record used to develop Figure 48 was applied.

The time history results were processed at each time step to obtain maximum inter-story drifts. Maximum drifts were also calculated using the procedure of NZS4203 for a response spectrum analysis, where the nonlinear drifts are added to the elastic drift. Figures 49 and 50 compare the results for the X and Z directions respectively. These drifts are at the centre of mass of the building.

In the X direction the maximum response spectrum analysis (RSA) drift was 0.68%, compared to the peak nonlinear time history (NLTH) value of 0.88%. In the Z direction, the response spectrum drift was 0.36% and the time history drift 0.51%. The RSA drifts are for $S_p = 0.67$, whereas the NLTH values are based on $S_p = 1.0$.

If the RSA drifts are adjusted for $S_p = 1.0$ the peak X value will be 15% higher than the time history value and the peak Z value 5% higher. This suggest a relatively close correlation between response spectrum results and time history results when the time history is scaled to match the spectrum.

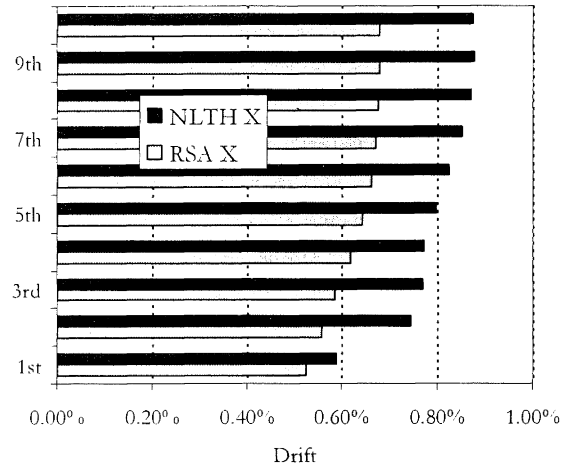

Figure 49. X (Coupled) Direction Drifts

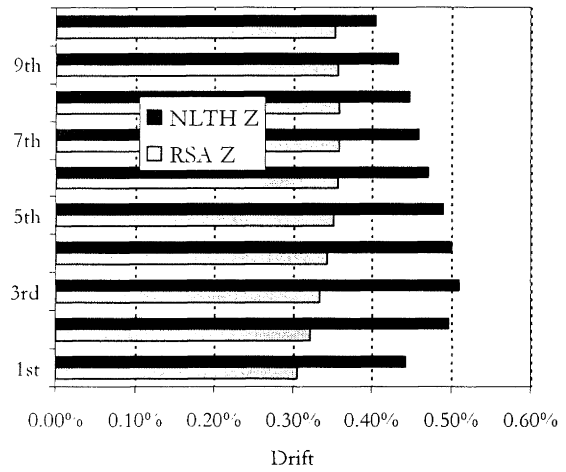

Figure 50. Z (Cantilever) Direction Drifts

Maximum component deformations in each wall are summarised in Table 10. For shear response, the maximum shear strain is 0.0032 in the X walls and 0.0031 in the Z walls. As the strength of the concrete plus steel is reached at a shear strain of 0.0045 and failure at 0.0075 there is a large margin of shear strength available.

The maximum gap opening, which corresponds to the plastic extension of the reinforcing, is used to estimate plastic rotation in each wall. Values are much higher in the X direction, 0.007 radians, than the Z direction, 0.002 radians, reflecting the shorter walls in that direction. The FEMA-356 limits for these walls would be 0.020 with a confined boundary and so the maximum flexural deformation is less than one-half the limit.

Table 10. Results for Spectrum Compatible Earthquake

Wall	Wall Length (m)	Maximum Shear Strain	Maximum Joint Opening (m)	Wall Plastic Rotation (radians)
X 1	3.500	0.0032	0.025	0.007
X 2	3.500	0.0024	0.020	0.006
X 3	3.500	0.0023	0.018	0.005
Z 1	10.000	0.0023	0.023	0.002
Z 4	4.500	0.0031	0.002	0.001
Z 5	4.500	0.0030	0.002	0.001

Coupling beam plastic rotations at each level are plotted in Figure 51. Plastic rotations are relatively constant with height, with a maximum value of 0.008 radians and a mean value of 0.007 radians. As FEMA allows plastic rotations up to 0.030 for diagonally reinforced coupling beams these beams provide a wide margin.

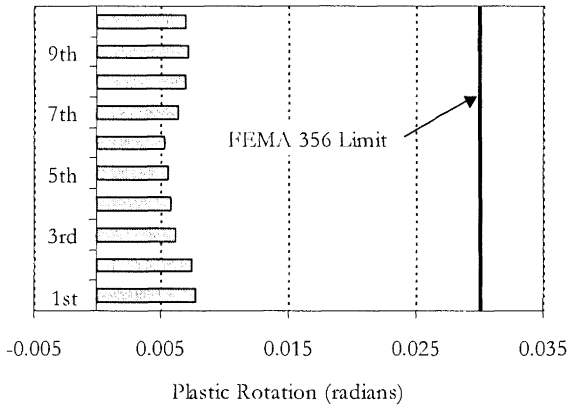

Figure 51. Coupling Beam Rotations

8.7.2 Scaled Suite of Time Histories

Although the current loadings code is non-prescriptive regarding time history selection, the draft code DR1170 [21] provides a detailed procedure for selecting and scaling a suite of time histories for nonlinear analysis.

The draft code has been used to scale the three time histories listed in Table 11 for an Intermediate Site with Z = 0.9. Of the three earthquakes, one is from a New Zealand site and the other two are from Mexico and Italy. None of the records are considered to contain the forward directivity effects associated with near fault motions and so they are suited for sites located more than 20 km from active faults.

The scaling procedure is such that the scaled motions envelope the target spectrum in the range $0.4T_1$ to $1.3T_1$ where T_1 is the fundamental period in the direction under consideration. For a building with well separated translational periods, such as this example, this results in different sets of scale factors in each direction.

In both directions, the primary component was the first of the two listed in Table 11 for each earthquake. In accordance with DR1170, the scaling factor computed for the primary component was also applied to the secondary component and both components were applied to the model concurrently.

Table 11. Earthquake Scaling Factors

Earthquake	Component	X Factor	Z Factor
Mexico, 1979	N08W	1.07	1.14
Delta	S82W	1.07	1.14
Italy, 1980	N00E	12.27	10.61
Bovino	N90E	12.27	10.61
Edgecumbe, 1987	N07W	2.27	1.68
Matahina D	N83E	2.27	1.68

Figure 52 plots the envelope of the three records compared to the target spectrum. The envelope provides a reasonable match over the period range for which scaling was performed but exceeds the target by a large margin outside this range, especially for shorter periods.

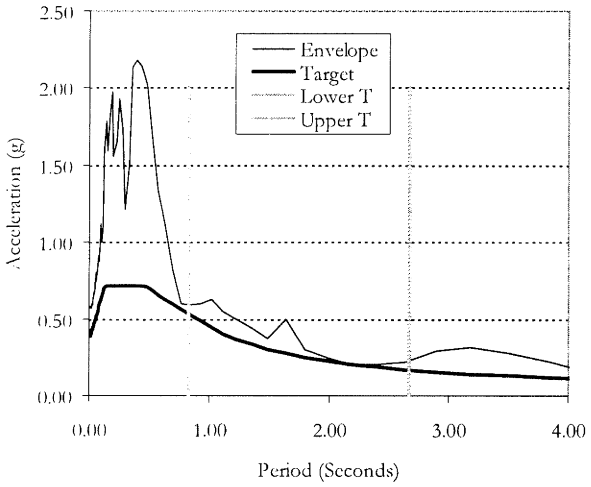

Figure 52. Envelope of Scaled Time Histories (X Direction)

Figure 53 plots the maximum drifts at each story in each direction, Table 12 lists maximum wall deformations and Figure 54 plots the coupling beam rotations. In all cases the results are the envelope values from the 12 analyses (3 earthquakes x 2 directions x 3 centre of mass locations).

As the building is symmetrical about one axis, only two eccentricity cases were analysed (+x, +z and –x, -z). Therefore, maximum results will not be obtained in all walls and symmetry is used to obtain envelope values. The actions in Walls 2 and 3 will each be equal to the maximum of either Wall 2 or Wall 3, and similarly for Walls 4 and 5.

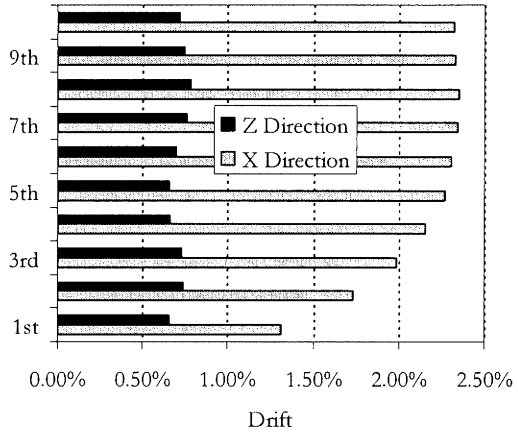

Figure 53. Scaled Time History Drifts

Table 12. Results for Scaled Time Histories

Wall	Wall Length (m)	Maximum Shear Strain	Maximum Joint Opening (m)	Wall Plastic Rotation (radians)
X 1	3.500	0.0057	0.052	0.015
X 2	3.500	0.0036	0.054	0.015
X 3	3.500	0.0053	0.082	0.023
Z 1	10.000	0.0035	0.046	0.005
Z 4	4.500	0.0063	0.003	0.001
Z 5	4.500	0.0068	0.003	0.001

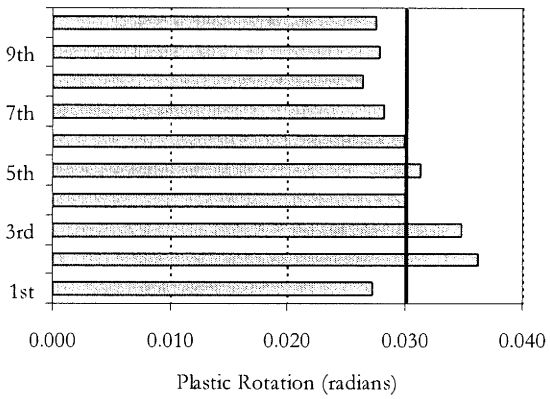

Figure 54. Coupling Beam Plastic Rotations

The maximum X drift is 2.35% and the maximum Z drift 0.78%. The maximum shear strain is 0.0057 in the X walls and 0.0068 in the Z walls. The probable shear strength of the wall (concrete plus steel) is reached at a shear strain of 0.0045 and so the shear stress in 4 of the 6 walls is sufficient to yield the shear steel. In walls 4 and 5, the shear stress at a strain of 0.0068 is close to the shear overstrength of the wall (0.0075) at which shear failure would be incipient.

The plastic rotations in the shorter walls, Walls 1 to 3, are 0.023, over the limit of 0.020 for this type of component. The maximum coupling beam plastic rotations, up to 0.036, exceed the limit of 0.030 for diagonally reinforced elements at three levels.

All results are much higher than for the evaluation using the spectrum compatible records. The structure performed well under the former records but is on the verge of failure under the records scaled according to DR 1170.

Figure 55 plots the maximum drifts for each earthquake and this shows very clearly that earthquake 3, which is the Matahina Dam record from the 1987 Edgecumbe earthquake, provides much higher drifts than the other two earthquakes, particularly in the X direction.

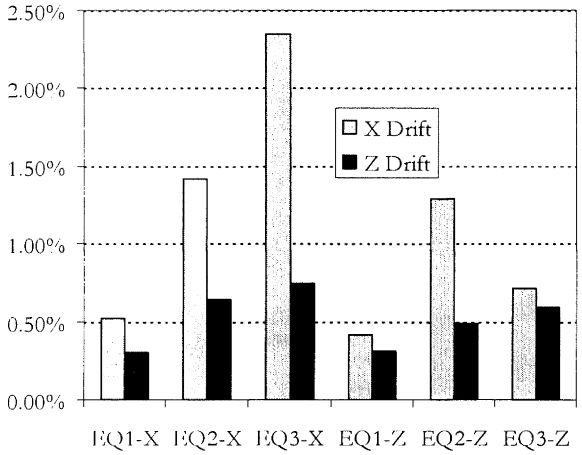

Figure 55. Drifts by Earthquake

Figure 56 plots the time history of roof displacement for EQ3-X, which produced the peak response. From successive peaks, the periodicity of response is extracted as approximately 3.50 seconds, well in excess of the 2.05 second elastic period.

The 5% damped acceleration response to the primary component of the Matahina Dam record is plotted in Figure 57 and compared to the target spectrum. The acceleration response is seen to increase from about 2.3 seconds to a peak at about 3.4 seconds. Although the acceleration peak is low compared to the short period peaks, it has a much more pronounced effect on the displacement spectrum, shown in Figure 58, because of the relatively long period.

When the wall softens and the period increases from 2.05 seconds to beyond 2.50 seconds, the structure attracts higher accelerations and the displacement response increases rapidly, as shown on the spectrum in Figure 58. The increased displacement further lengthens the period and so the displacement continues to increase.

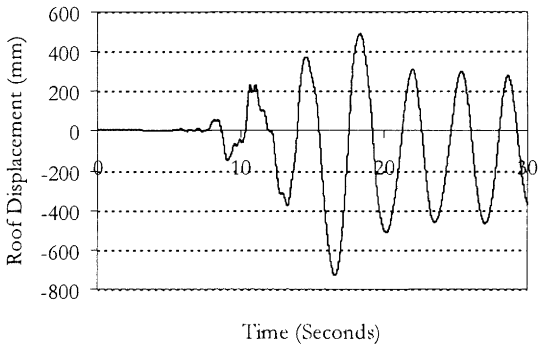

Figure 56. X Response to Matahina

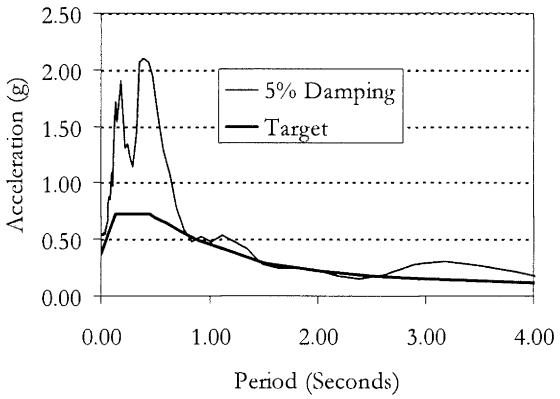

Figure 57. Matahina N07W 5% Acceleration Spectrum

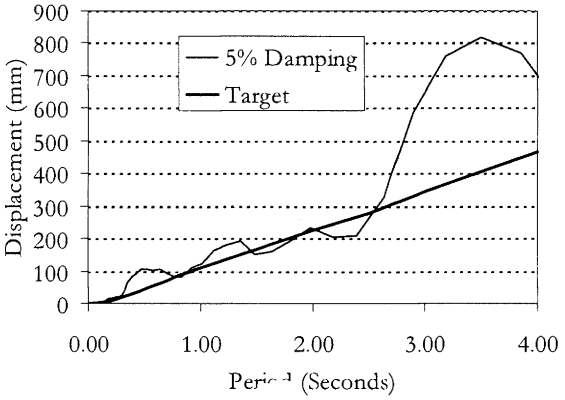

Figure 58. Matahina N07W 5% Displacement Spectrum

The well defined first mode response in Figure 56 permits the effective damping in the system to be estimated. The peak roof displacement from this analysis is 744 mm. Assuming a linear profile of displacement with height, the displacement at the centroid, 2H/3, will be 496 mm. At 5% damping, the spectral displacement at T = 3.5 seconds is 795 mm (Figure 58), which indicates that the damping is higher than 5%. By generating spectra for various values of viscous damping it can be determined that a ratio of 13.5% produces 503 mm displacement. At a period of 3.50 seconds the Rayleigh

coefficients in the model provide 7% viscous damping and so the hysteretic damping is equivalent to an increase of 6.5% in the effective damping.

8.8 Evaluation of Performance

Table 13 summarises the maximum deformations in each wall for the spectrum compatible earthquake, the DR 1170 suite of time histories and the DR 1170 suite with Earthquake 3 (Matahina) excluding from the processing. For the evaluation of performance, it is assumed that the DR 1170 records scaled for S_p = 1.0 represents the upper level earthquake and that Collapse Prevention (CP) criteria apply. In terms of these criteria:

1. The shear strains are less than the CP limit of 0.0075 for all walls although they reach a level close to this limit (0.0068) for the full DR 1170 set.

2. The maximum wall plastic rotations exceed the CP limit of 0.020 radians under the full DR 1170 set (0.023).

3. Coupling beam plastic rotations exceed the CP limit of 0.030 radians under the full DR 1170 set.

As discussed above, the high deformations are caused by the energy input of one particular record and when this wall is excluded all deformations are within CP limits. However, even excluding EQ 3 the shear strain in Wall 1 exceeds the nominal strength (strain limit 0.0045).

Table 13. Evaluation of Structure

	Spectrum Compatible	DR 1170	DR 1170 Excluding EQ 3
X Shear Strains			
Wall 1	0.0032	0.0057	0.0047
Walls 2/3	0.0024	0.0053	0.0031
Z Shear Strains			
Wall 1	0.0023	0.0035	0.0026
Walls 4/5	0.0031	0.0068	0.0041
X Plastic Rotations			
Wall 1	0.0070	0.0148	0.0147
Walls 2/3	0.0058	0.0233	0.0122
Coupling Beams	0.0077	0.0363	0.0210
Z Plastic Rotations			
Wall 1	0.0023	0.0046	0.0028
Walls 4/5	0.0005	0.0007	0.0007

As the earthquake input continues to increase the overall structural deformations increase and so it is inevitable that plastic rotations will eventually exceed the limits. However, the wall was designed using capacity design principles which are intended to prevent brittle (shear) failure even at high deformations. The capacity design procedure of NZS3101 uses plastic hinge overstrength and a dynamic magnification factor, ω_v, to develop upper bound shear forces and is intended to ensure that the nominal shear strength (concrete + steel) is not exceeded.

The shear strength limit is defined at a shear strain of 0.0045 and Table 13 shows that this limit is exceeded in all walls except Wall 1 Z under the full set of DR 1170 records. These walls are relying on shear steel overstrength and strain hardening to maintain their integrity. The capacity design procedure is not protecting the walls at these very high deformations. This suggests that the dynamic magnification factor, ω_v, may be too low for this particular wall configuration.

9 CONCLUSIONS

This paper has described the development of a finite element procedure for the nonlinear static and dynamic analysis of shear wall structures of arbitrary configuration. The procedure is based on macro modelling which produces complete building models of sufficient simplicity to permit nonlinear time history analysis within a design office environment.

Model characteristics are developed from a combination of the principles of engineering mechanics and experimental data and implemented into an existing nonlinear analysis computer program. Comparisons with experimental results show that the procedure can capture the overall strength and hysteretic characteristics of a range of wall types with and without openings.

The macro modelling procedure does not explicitly model all components of response and so empirical criteria, available in published guidelines, are used to evaluate performance. However, the model formulation is such that further development could permit more specific evaluation of wall components.

The procedure was applied to a prototype building designed to current codes and this showed excellent performance when evaluated for a time history compatible with the design condition. However, when the same building was evaluated under a suite of records scaled according to draft provisions of the new code the building was on the point of incipient failure due to excessive shear stresses and coupling beam deformations.

The analyses on the full building raised questions about time history scaling procedures and the adequacy of the dynamic magnification factors in our current and proposed codes. These aspects will be among the subjects of continued study of the performance of shear wall structures.

10 ACKNOWLEDGMENTS

Valuable discussions with many engineers at Holmes Consulting Group, particularly Graham Voysey, Des Bull, Jonathan Chambers and Bill Tremayne, are gratefully acknowledged. Thanks are also due to my fellow shareholders for their financial support of these development efforts.

11 REFERENCES

1. Blakeley R.W.G., Cooney, R.C. and Megget, L.M. (1975). "Seismic Shear Loading at Flexural Capacity in Cantilever Wall Structures", *Bulletin of the New Zealand National Society for Earthquake Engineering*, Vol. **8**, No. 4, December.

2. "ATC Seismic Evaluation and Retrofit of Concrete Buildings", ATC-40, *Applied Technology Council*, California, November, 1996.

3. Hui Wu and Bing Li, (2003). "Investigating the Load Paths of RC Shear Walls with Openings Under Reversed Cyclic Loadings", *Pacific Conference on Earthquake Engineering, New Zealand.*

4. "RAM Perform-3D, Version 1.10 User Guide" (2000). *RAM International LLC.*

5. "Concrete Structures Standard : Part 1 - The Design of Concrete Structures", NZS 3101:Part 1:1995, *Standards New Zealand*, 1992.

6. Habibullah, A. (1994). "ETABS Three Dimensional Analysis of Building Systems USER'S MANUAL", Version 6.0, *Computers and Structures Inc*, Berkeley, CA, October.

7. Paulay. T. and Priestley, M.J.N., (1992). "Seismic Design of Reinforced Concrete and Masonry Buildings", *John Wiley & Sons.*

8. "Prestandard and Commentary for the Seismic Rehabilitation of Buildings", *FEMA-356, Federal Emergency Management Agency*, Washington D.C. November, 2000.

9. "Repair of Earthquake Damaged Concrete and Masonry Wall Buildings", *FEMA-306, 307 and 308, Federal Emergency Management Agency*, Washington D.C. May, 1999.

10. Mondkar, D.P. and Powell, G.H. (1979). "ANSR II Analysis of Non-linear Structural Response User's Manual", *EERC 79/17, University of California*, Berkeley, July.

11. Kelly, T.E., Button, M.R., Mayes, R.L. (1984). "Seismic Evaluation of Reinforced Masonry Walls", *Structural Engineering in Nuclear Facilities, ASCE Conference,* Raleigh, North Carolina, September.

12. Kelly, T.E. and Chambers, J.D. (2000). "Analysis Procedures for Performance Based Design", *12th World Conference on Earthquake Engineering,* Auckland, New Zealand.

13. Fenwick, R. and Bull, D. (2001). "Stiffness of Structural Walls for Seismic Design", *SESOC Journal*, Vol. **14,** No 2, September. *Structural Engineering Society of New Zealand.* (Also Discussion by N. Priestley and T. Paulay, and Authors' Reply, Vol. **15**, No. 1, April 2002).

14. Fenwick, R. and Bull, D. (2000). "What is the Stiffness of Reinforced Concrete Walls?" *SESOC Journal*, Vol. **13,** No. 2, September. *Structural Engineering Society of New Zealand.*

15. Paulay, T. and Goodsir, W.J. (1985). "The Ductility of Structural Walls", *Bulletin of the New Zealand National Society for Earthquake Engineering*, Vol. **18**, No. 3, September.

16. Yanez, F.V., Park, R. and Paulay, T. (1991). "Seismic Behaviour of Reinforced Concrete Structural Walls and Regular and Irregular Openings", *Proceeding Pacific Conference on Earthquake Engineering*, New Zealand, November.

17. Mander, J.B., Panthaki, F.D. and Kasalanti, A. (1994). "Low Cycle Fatigue Behaviour of Reinforcing Steel", *Journal of Civil Engineering Materials, ASCE*, **6** (4).

18. Priestley, M.J.N. (2000). "Performance Based Seismic Design", *12th World Conference on Earthquake Engineering*, Auckland, New Zealand.

19. Bull, D. and Brunsdon, D. (1998). "Examples of Concrete Structural Design to New Zealand Standard 3101", *Cement & Concrete Association of New Zealand*, August.

20. "Code of Practice for General Structural Design and Design Loadings for Buildings", NZS 4203:1992, *Standards New Zealand*, 1992.

21. Draft AS/NZS 1170.4 Standard: "Structural Design Actions – Part 4 Earthquake Actions", *Standards New Zealand*, Pre-Ballot Draft 1, 2004.